https://doi.org/10.5194/egusphere-2026-4644
Preprint. Discussion started: 9 September 2026

Determination of weather-driven trends of atmospheric emissions, concentrations and deposition over Europe during the last decades

Florian Couvidat[1], Antoine Guion[1], Victor Lannuque[1], Palmira Messina[1], Elsa Real[1], Gaël Descombes[1], Pauline Buysse[2,3], Augustin Colette[1], and Raia Silva Massad[2]

[1]INERIS, Institut National de l'Environnement Industriel et des Risques, Parc Technologique ALATA, Verneuil-en-Halatte, 60550, FranceA
[2]Université Paris-Saclay, INRAE, AgroParisTech, UMR ECOSYS, 91120, Palaiseau, France
[3]Now at: INRAE-Institut Agro, UMR SAS, 35000, Rennes, France

Correspondence: Florian Couvidat (florian.couvidat@ineris.fr)

Abstract.

The dependency of emission and atmospheric physicochemical processes on various meteorological drivers are often not completely accounted for by 3D air quality models. In order to tackle this issue, the present study assesses weather-driven trends in atmospheric emissions and air quality in Europe over 1990–2022 using an enhanced version of the CHIMERE chemical transport model. The model includes meteorology-dependent anthropogenic emissions, varying 8-day leaf area index from satellite data over the whole period, and updated parameterizations for deposition as well as soil and biogenic emissions. Simulations performed with constant anthropogenic emission practices indicate significant increases in biogenic VOC, ammonia, and soil NOx emissions. In contrast, emissions decrease for the residential sector and road traffic NOx, due to warmer temperatures reducing heating and cold-start emissions.

Ozone annual concentrations show regionally contrasting trends, with increases in southern Europe but decreases in northern regions due to enhanced deposition linked to vegetation changes. Significant increases, driven mainly by rising temperatures and solar radiation, are simulated for SOMO35 and AOT40c, with population-weighted trends of 0.5%/yr and 0.69%/yr, corresponding to overall increases by 18% and 22% over the 1990–2022 period, respectively. Fine particulate matter generally declines (population-weighted trend of -0.03 μg/m^3/yr, +0.95 μg/m^3 over the period), despite increases in secondary organic aerosols and bioaerosols. Reduced nitrogen deposition also increased (+3.9 kT/yr, around +4.8% over the period) due to increases in ammonia gas-phase fraction and emissions.

1 Introduction

Atmospheric pollution results from the emissions of biogenic and anthropogenic pollutants in the atmosphere combined with their transport and the formation of secondary pollutants through chemical reactions. This pollution is strongly affected by weather conditions: wind speed and turbulence influence transport; precipitations influence wet deposition; temperature and

https://doi.org/10.5194/egusphere-2026-4644
Preprint. Discussion started: 9 September 2026

humidity influence the chemistry or the formation of aerosols as well as emissions and deposition. All of these variables are expected to evolve with climate changes with strong regional variations (Coelho et al., 2021; He et al., 2024).

The evaluation of the impact of climate change on air quality is generally based on the use of Chemical Transport Models (CTM) driven by meteorological or climate fields (Jacob and Winner, 2009). Modeling studies generally indicate a climate penalty leading to an increase in tropospheric ozone concentrations (Meleux et al., 2007; Tagaris et al., 2007; Zeng et al., 2008; Katragkou et al., 2011; Fiore et al., 2012; Colette et al., 2013; Eyring et al., 2013; Gao et al., 2013; Rasmussen et al., 2013; Stowell et al., 2017; Guion et al., 2023).

Simulation results are more contrasted on the influence of climate change on particulate matter (PM) concentrations. Climate change can lead to more severe PM episodes from wildfires (Venäläinen et al., 2014a; Jones et al., 2022, 2024) or to an increase in Saharan dust outbreaks toward Europe (Cuevas-Agulló et al., 2024). Several modeling studies reported an increase in Secondary Organic Aerosol (SOA) concentrations due to climate change linked to an increase in biogenic emissions (Heald et al., 2008; Lin et al., 2016; Cholakian et al., 2019). On the other hand, Secondary Inorganic Aerosol (SIA) concentrations are predicted to decrease with climate change due to temperature increases that inhibit nitrate formation (Heald et al., 2008; Cholakian et al., 2019).

One common limitation of most air quality studies is that the direct effect of temperature on anthropogenic emissions is not considered. With constant anthropogenic practices, climate change can favor ammonia emissions (increase in emissions by 42% reported by Sutton et al. (2013) for a 5 °C warming) and emissions from solvent use and gasoline evaporation (Wu et al., 2024). On the contrary, climate change can lead to a decrease in emissions from residential heating by reducing energy consumption and from road traffic by influencing cold-start emissions (Grange et al., 2019).

The objective of this study is to determine the weather-driven trends on air quality in Europe during the last decades by considering the dependency of emission and atmospheric physicochemical processes on drivers (including different meteorological variables, the LAI vegetation index and the deposition velocity) with state-of-knowledge parameterizations. Weather-driven trends for the concentrations of major atmospheric pollutants (O_3, NO_2 and PM) and atmospheric deposition of eutrophying and acidifying are determined by performing air quality simulations over the 1990-2022 period. To our knowledge, no studies have previously investigated to such an extent the effect of meteorological changes on both emissions and air quality over long periods. This study therefore provides valuable insights into the links between climate change, emissions and air quality.

2 Method

Simulations are based on a modified version of CHIMERE v2020r1 (Menut et al., 2021) in which the following developments were made in order to better represent the effect of meteorological variables on air quality in a context of climate change:

- Biogenic VOC emission calculations are revised in order to implement a multi-layer canopy module, instead of the standard "big leaf" approach used by CHIMERE v2020r1 (MEGAN model, Guenther et al., 2012). This module accounts for the effects of solar radiation, leaf area index (LAI), soil moisture (SM), leaf temperature (calculated with a thermal

https://doi.org/10.5194/egusphere-2026-4644
Preprint. Discussion started: 9 September 2026

balance as a function of ambient temperature, solar radiation, relative humidity and soil moisture). The developments are described in sect. 2.1.1.

- Following Vida et al. (2024), emissions of fungal spore particles are added. Emissions are calculated as function of LAI and specific humidity. The developments are described in sect. 2.1.1.
- Soil NOx emissions are computed with the parameterization of Yienger and Levy (1995) which accounts for the effect of soil temperature, soil moisture, precipitations and LAI. The developments are described in sect. 2.1.3.
- The dry deposition scheme is revised in order to harmonize calculations with the biogenic emission module (as described in sect. 2.1.2). Especially, the new deposition module accounts for the effects of solar radiation, LAI, soil moisture, leaf temperature and several turbulence parameters (such as friction velocity and the aerodynamic resistance).
- Several dynamic parameterizations on anthropogenic emissions have been implemented to account for the effect of temperature on the use of heating appliances (assuming that this usage decreases during warmer conditions, sect. 2.1.6), traffic emissions (sect. 2.1.7) and on volatile chemical product emissions (sect. 2.1.7). Agriculture ammonia emissions (sect. 2.1.4) from livestock and fertilizer usage are also calculated as a function of turbulence parameters, soil wind speed, air temperature, soil temperature, leaf temperature, soil moisture and LAI.

To disentangle the influence of meteorological variability, emissions from sectors and pollutants lacking dynamic parameterization are taken from an emission inventory that does not include interannual changes. Monthly and hourly emissions are derived from annual totals using CAMS-TEMPO v4.1 (Guevara et al., 2021). For this purpose, we use the CAMS-REG-AP inventory for the year 2018 (version v5.1_REF2.1) (Kuenen et al., 2022). For sectors and pollutants for which a dynamic parameterization is used, the calculated anthropogenic emissions are constrained to reproduce the annual emissions provided for 2018 (selected as a reference year) by the emission inventory or, in the case of agricultural NH_3 emissions, by the official reported emission provided by countries in 2024 on the the Centre on Emission Inventories and Projections (CEIP).

Simulations are performed for the 1990-2022 period over a $0.25° \times 0.25°$ domain covering Europe. Emission calculations and CHIMERE simulations are performed using meteorological data from the ERA5 reanalysis (Hersbach et al., 2020).

Several results are presented in this study for the area referred to as "EUR", representing the countries from the European Union (EU27) together with Norway, Switzerland and the United Kingdom. Dynamic NH_3 emissions are only considered for EUR countries in order to use the official reported emissions provided by countries in 2024. For other countries, NH_3 emissions are taken from the emission inventory without interannual variations.

2.1 Model development

2.1.1 Biogenic VOC and fungal spore emissions

CHIMERE v2020r1 currently computes biogenic emissions based on the MEGAN v2.1 algorithm (Guenther et al., 2012) that has been embedded in the code. Following Henrot et al. (2017), a "big-leaf" approach is used where vegetation is represented

https://doi.org/10.5194/egusphere-2026-4644
Preprint. Discussion started: 9 September 2026

by a single canopy level. The code also uses the air temperature at 2 meters above ground instead of the leaf temperature and does not account for the effect of soil humidity on isoprene emissions. As these assumptions could strongly affect the response of the model to changes in meteorological parameters, a multi-layer canopy module was implemented in CHIMERE.

The canopy is discretized into several layers (referred to as N_{layers}). For each level, the temperature of sunlit and shaded leaves as well as the photosynthetic photon flux density (PPFD) are computed with the approach described by Müller et al. (2008). The emission flux $F_{v,i,layer}$ is then computed with the following formulae for the different types of vegetation defined by Müller et al. (2008) (needleleaf evergreen, needleleaf deciduous, broadleaf evergreen, broadleaf deciduous, shrubs, grass, crops):

$$F_{v,i,layer} = EF_{v,i} \cdot C_{CE,v,i} \cdot \gamma_{SM,i} \cdot \gamma_{age} \cdot \gamma_{CO2,i} \cdot \Delta LAI_{v,layer} \cdot \gamma_{PT,v,i,layer} \quad (1)$$

with v a specific type of vegetation, i the species, $EF_{veg,i}$ the emission factor at standard conditions (conditions for which emission factors are measured), Δ $LAI_{v,layer}$ the fraction of LAI in the canopy layer. $\gamma_{SM,i}$, γ_{age}, $\gamma_{CO2,i}$ are the emission activity factors accounting for soil moisture, leaf age and CO_2 concentrations, respectively. $\gamma_{PT,v,i,layer}$ accounts for both the effect of PPFD and leaf temperature. γ_{age}, $\gamma_{CO2,i}$ and $\gamma_{PT,v,i,layer}$ are computed with the parameterizations of Guenther et al. (2012). In order to calculate $\gamma_{CO2,i}$ (applied on isoprene only), the yearly concentrations of CO_2 measured at Mauna Loa are used (Lan and Keeling, 2024). $\gamma_{SM,i}$ is computed as in Müller et al. (2008) by using the soil moisture at different depths provided by the ERA5 reanalysis and the gridded wilting point dataset provided by the International Geosphere-Biosphere Program Data and Information System (IGBP-DIS) at a resolution of 30 arcsec (Global Soil Data Task, 2000).

In order to use Eq. 1, LAI must be distributed vertically, temporally, and by vegetation type. The vertical distribution can be obtained by using Leaf Area Density (LAD) functions. LAD functions for the different types of forests are taken from Bonan et al. (2018). The LAI is assumed to be vertically uniform for the other types of vegetation types (grass, shrubs and crops). Gridded LAI data, estimated from the MODIS satellite instruments, are used to provide information on the spatiotemporal distribution of LAI. Since the LAI estimate is provided for total vegetation, these gridded data were combined to the generic LAI evolution functions by type of vegetation proposed by Emberson et al. (2000). These functions are traditionally used within CHIMERE to compute deposition fluxes by type of vegetation. Furthermore, the fraction of a vegetation type inside a cell was estimated using the Corine Land Cover (CLC) dataset (CLMS, 2020).

Two LAI satellite datasets are considered in our study. The first dataset (referred to as "default LAI" hereafter) consists in high spatiotemporal LAI (30 arcsec every 8 days) generated from MODIS instrument for year 2018 with the method of Yuan et al. (2011). Alternatively, the HiQLAI database (Yan et al., 2024) has a 5 km resolution with data every 8 days and covers the period 2000-2022. This database was completed by the GlobMAP database (Liu et al., 2012) in order to cover the whole simulation period (1990-2022).

Finally, three sources of emission factors were considered: the generic EF of MEGAN v2.1 by vegetation types provided by Guenther et al. (2012), the EF by vegetation types and ecoregions provided within MEGAN v3.2 (Guenther, 2024) and the EF used within the ORCHIDEE model (Messina et al., 2016).

https://doi.org/10.5194/egusphere-2026-4644
Preprint. Discussion started: 9 September 2026

Vida et al. (2024) simulated fungal spore concentrations with CHIMERE by using the parameterization of Heald and Spracklen (2009) to estimate the emissions. The authors evaluated the model results by comparing concentrations with estimates of spore concentrations based on polyol measurements in France. They showed that the model could accurately reproduce the fungal spore concentrations at most stations in France. Therefore, fungal spore emissions are here calculated with the same method. The fungal spore number emissions $F_{H\&S}$ (in #/m^2/s) are calculated with the following equation:

$$F_{H\&S} = 30\,867 \times LAI \times qv \tag{2}$$

with qv the specific humidity (in kg/kg). Fungal spore emissions are assumed to have a density of 1000 kg/m^3 and an aerodynamic diameter of 3 μm.

2.1.2 Dry deposition

Several modifications were made to improve the calculation of deposition velocities based on the resistance approach of Wesely (1989). CHIMERE v2020r1 uses the cell averaged friction velocity u* regardless of the land-use categories. The calculation of u* has been revised to account for the roughness length (z_0) of the different land-uses categories. Following Simpson et al. (2012), the friction velocity u* is recalculated for each land-use categories based on z_0 and the wind speed of the third layer of the Integrated Forecast System (IFS) meteorological model (corresponding to an altitude of 50 m, a height where wind speed is not influenced by the underlying terrain):

$$u^* = \frac{k \times U(z_{ref})}{ln\left(\frac{z_{ref}-d}{z_0}\right) - \psi_M\left(\frac{z_{ref}-d}{L}\right) + \psi_M\left(\frac{z_0}{L}\right)} \tag{3}$$

with k the von Karman constant (=0.41), z_{ref} the height of the third vertical layer of the meteorological model, U(z_{ref}) the wind speed of the third vertical layer, d the displacement height, L the Obukhov length and ψ_M the stability functions for momentum. ψ_M is calculated as in IFS (ECMWF, 2016). The values of z_0 and d are taken from Simpson et al. (2012).

Deposition velocities on vegetation are calculated based on Clifton et al. (2020). Stomatal fluxes are calculated according to Müller et al. (2008). With this changes, the current version of the dry deposition model for stomatal conductance includes the effect of soil moisture in addition to the other parameters already included in CHIMERE v2020r1 (temperature factor, irradiance, leaf-to-air vapor pressure deficit). The temperature factor is also calculated using the leaf temperature instead of air temperature. While CHIMERE v202r1 uses the LAI functions from Emberson et al. (2000) to calculate deposition fluxes, deposition velocities are based, in our study, on the LAI redistributed on vegetation classes (see Sect. 2.1.1) to homogenize the LAI data used for both deposition and biogenic emissions.

2.1.3 Soil NO emissions

The parameterization of Yienger and Levy (1995) is implemented in CHIMERE to compute NO emissions from soils (F_{NO}):

$$F_{NO} = f_{w/d}\left(T_{soil}, A_{w/d}(\text{veg})\right) \times P(precipitation) \times CR \tag{4}$$

https://doi.org/10.5194/egusphere-2026-4644
Preprint. Discussion started: 9 September 2026

with $f_{w/d}$ the response of emissions under dry (d) and wet (w) conditions to the soil temperature (T_{soil}) and depending on $A_{w/d}(veg)$ a factor depending on the vegetation type, P (precipitation) is a factor representing pulse emissions due to precipitation and a reduction factor (CR) to account for NOx uptake by vegetation inside the canopy.

For agricultural soils, Yienger and Levy (1995) proposed to use an emission factor due to fertilization (EF_{NO}) representing a 2.5% annual loss of the amount of nitrogen and applied to each grid cell such as:

$$A_{w/d}(\text{crops}) = A_{w/d}(\text{grassland}) + S \times N_{cumul} \tag{5}$$

with N_{cumul} the accumulated amount of N in soils due to fertilizer applications and S the scaling factor for fertilizer volatilization determined for each grid cell. Yienger and Levy (1995) normally uses the monthly application rate but, following Yan et al. (2005), using N_{cumul} calculated with daily application of fertilizers and a lifetime of 4 months was preferred. Instead of forcing S over each grid cell in our study, a single value of S is determined for the whole domain and is scaled for year 2018. The computation of daily application is presented in Sect. 2.1.5.

2.1.4 Ammonia emissions

NH_3 emissions from housing, storage and grazing are temporalized according to Skjøth et al. (2011) to take into account the impact of temperature and wind speed. For each country, the emissions are calibrated to respect the emissions reported on CEIP for year 2018.

NH_3 emissions due to fertilizer applications ($F_{NH3,fert}$) are computed offline with the parameterizations of Massad et al. (2010) such as:

$$F_{NH3,fert} = S_c \frac{1}{R_a} \frac{\chi_g/R_g + \chi_c(\chi_s,\chi_g)/R_b}{R_a^{-1} + R_g^{-1} + R_b^{-1}} \tag{6}$$

with R_a the aerodynamic resistance, R_b the quasi laminar boundary resistance for vegetation, R_g the quasi laminar boundary resistance for the ground, χ_c the compensation point calculated with χ_s and χ_g the stomatal and ground layer compensation point calculated as a function of fertilizer applications. The resistances, determined for crops, are calculated with the resistance scheme of CHIMERE. S_c is a scaling factor determined for each country to respect the 2018 emission level of NH_3 emissions from fertilizer applications.

2.1.5 Distribution of fertilizer applications

To compute NH_3 and soil NOx emissions, fertilizer applications have to be spatially and temporally distributed. The amounts of inorganic and organic fertilizers per country are extracted from the FAOSTAT website (https://www.fao.org/faostat/ ; Last access in August 2024) and are spatialized according to the agricultural land-use. Temporalization is performed according to the temperature sums and the gaussian distributions of Skjøth et al. (2011).

$$R_{fert,type,t} = Fert_{type} \sum_{i}^{n_{type}} f_i \frac{exp\left(\frac{(t-\mu_i)^2}{-2\sigma_i}\right)}{\sigma_i\sqrt{2\pi}} \tag{7}$$

https://doi.org/10.5194/egusphere-2026-4644
Preprint. Discussion started: 9 September 2026

with the "type" index referring to the type of fertilizers used (inorganic or organic), t the julian day of the year, $R_{fert,type,t}$ daily applications of fertilizers, n_{type} the number of sub-sectors corresponding in Skjøth et al. (2011) (subsectors "Spring application of fertilizer" and "Summer application of fertilizer" are used for inorganic fertilizers, subsectors "Spring application of manure on bare soil", "Application of manure on crops", "Summer application of manure", "Autumn application of manure" are used for organic fertilizers), f_i corresponds to the fraction of the fertilizer used in the sub-sector, μ_i corresponds to the day when the gaussian function reaches its maximum (computed as a function of temperature sums) and σ_i is the spread of the gauss function. f_i and μ_i are directly extracted from Skjøth et al. (2011). σ_i in Skjøth et al. (2011) ranges from 9 days (for application of manure) to 30 days. Using σ_i=9 days strongly limits the spread of the gauss function and lead to specific period with considerable NH_3 emissions (whereas NH_3 is generally present during large period in spring). σ_i was chosen equal to 30 to avoid this issue.

2.1.6 Residential heating emissions

Temperature does not directly influence the emissions factors for residential emissions, but it can affect activity through energy consumption for heating. Guion et al. (2025) proposed that the Heating Degree Days (HDD) approach (assuming that residential emissions are directly proportional to the difference between the outdoor temperature and a comfort temperature T_b) can be used to include the effect of colder temperature on emissions. HDDs daily factors are calculated with:

$$HDD_{i,j,d} = max(T_b - T_{2m,i,j,d}, 0) \tag{8}$$

with i the longitude index, j the latitude index, d the day index, T_{2m} the daily temperature at 2 meters above ground. Based on HDDs, residential emissions from wood burning ($F_{RWB,i,j,d,n}$) for the species n can be calculated as follows:

$$F_{RWB,i,j,d,n} = \left(\frac{f_{RWB,n}}{N_{days}} + (1 - f_{RWB,n}) \frac{HDD_{i,j,d}}{\sum_k HDD_{i,j,k}} \right) \times E^{2018}_{RWB,i,j,n} \tag{9}$$

with N_{days} the number of days in a year, $f_{RWB,n}$ the fraction of household activities that are not sensitive to temperature variations (e.g. cooking and water heating) in the NFR emission sector C "other stationary combustions" in the Gridding Nomenclature for Reporting ($GNFR_C$), and $E^{2018}_{RWB,i,j,n}$ the annual emission of the cell for 2018 as reference year.

2.1.7 NOx and NMVOC emissions from road trafic and solvent use

Although NO_x emissions from diesel vehicles can also be strongly dependent on ambient temperature, this effect is generally not taken into account in emission inventories. According to Grange et al. (2019), it could lead to an underestimation of emissions by 38%. However, the effect of temperature on diesel NOx emissions strongly depends on the type of vehicle. NOx emissions from EURO 6 vehicles may exhibit a low temperature dependence according to Grange et al. (2019). For the purpose of our study, the emission correction based on the ambient temperature of Wærsted et al. (2022) was used. This correction was determined by studying the bias in NO_2 concentrations simulated with the uEMEP model (Mu et al., 2022) at stations in Norway. The correction was applied to the GNFR F2 sector (from road transport – diesel exhaust) for NOx. It should probably

https://doi.org/10.5194/egusphere-2026-4644
Preprint. Discussion started: 9 September 2026

be adjusted country by country based on the fleet composition of diesel vehicles, but due to the lack of data, the correction was assumed to be representative and valid for all of Europe. No correction was applied to the other pollutants.

Finally, the temperature dependence of non-methane volatile organic compounds (NMVOC) from gasoline evaporation and solvent use was calculated according to the parameterizations of Wu et al. (2024).

2.2 Model evaluation

An ensemble of simulations were performed for year 2018 in order to compute biogenic emissions using different biogenic EF (MEGAN 2.1, MEGAN 3.2 and ORCHIDEE) and different LAI database (Yan et al. (2024) and HiQLAI). The map of biogenic emissions of total VOC, isoprene, monoterpene and sesquiterpenes calculated with different EF database are shown in the supplementary materials (Fig. S1 to S4). The effect of the use of the canopy module on biogenic is illustrated by Fig. S5.

The effect of the different model improvements on performance is also assessed by comparisons to in-situ measurements of surface concentrations reported by the European air quality observation network AQ e-Reporting (EEA, 2023). A comprehensive evaluation of biogenic emissions and model performance is provided in the Supplementary Material (Sections S1 and S2), including the temporal evolution of observed and simulated concentrations (Fig. S6 to S8) as well as a range of performance metrics (Fig. S9 to S13).

Concerning biogenic emissions, much higher terpene emissions are obtained with MEGAN 3.2 compared to the Big-Leaf approach of CHIMERE v2020r1. These results are consistent with other studies over Europe that indicated a strong underestimation (by a factor 3) of terpene emissions (Jiang et al., 2019; Ciccioli et al., 2023). Based on these studies, Wang et al. (2024b) increased the emissions of monoterpenes and sesquiterpenes simulated by CHIMERE v2020r1 by a factor 3. The authors obtained significantly improved simulation results for summertime PM2.5 and organic aerosols, as evidenced by comparisons with measurements. According to our results, MEGAN 3.2 should be considered the most up-to-date and realistic EF database.

The new CHIMERE version developed in this study has generally better scores than CHIMERE v2020r1 for PM concentrations (RMSE for PM10 reduced from 9.0μg/m^3 to 8.1μg/m^3 and correlations increase from 0.54 to 0.62) and similar scores for O_3 (RMSE slightly reduced from 16.4 and 16.2 μg/m^3) and NO_2 (RMSE is sightly reduced from 5.11 to 4.9 μg/m^3 but the correlation slightly decreases from 0.61 to 0.60) concentrations.

2.3 Determination of weather-driven trends and drivers

Weather-driven trends (trends calculated over the simulation period that consider only the effect of weather conditions and assumed constant practices) are calculated cell by cell for the period 1990-2022 using the Sen-Theil approach. p-values are calculated with the Mann-Kendall trend test using the "pyMannKendall" python library (Hussain and Mahmud, 2019). Following several studies (e.g. Houssami et al. (2010); Lin et al. (2022); Sillanpää et al. (2022)), trends are classified as "highly significant", "significant" and "slightly significant" for p-values$<$0.01, 0.01$\leq$p-values$<$0.05 and 0.05$\leq$p-values$<$0.1, respectively.

In order to determine the drivers (including different meteorological variables, the LAI vegetation index and the deposition velocity), annual concentrations or metrics (C) are expressed for each cell of the domain as a multilinear combination of the

https://doi.org/10.5194/egusphere-2026-4644
Preprint. Discussion started: 9 September 2026

annual averages of several selected meteorological variables (P_i) using a multilinear regression such as:

$$C = \text{residues} + \sum_{\text{i=met variables}} \alpha_i \times P_i \quad (10)$$

The selected variables for NO_2 are: temperature at 2m (T_{2m}), shortwave downward radiation (Solar), relative humidity at 2m (RH_{2m}), wind velocity (Wind) of the first vertical model (at around 10 m), LAI, precipitation (Precip) and the planetary boundary layer height (PBL). Ozone dry deposition velocities (v_d), directly extracted from CHIMERE, were added to the list of meteorological variables for O_3. In order to reach high correlation of the multilinear models for PM and deposition of acidifying and eutrophying compounds, cloud liquid water content (LWC) integrated over the first five layers was added to the list of variables to represent aqueous-phase oxidation of SO_2 into sulfate and wind velocity was replaced by the annual averages of southerly, northerly, westerly, easterly wind velocities.

The variables were selected to avoid high correlation between them. The maps of interannual trends for meteorological variables and the autocorrelation matrix between the considered variables are illustrated in the supplementary materials (Fig. S14 to S16). As a result, relative humidity was preferred to specific humidity to avoid autocorrelation between the annual averages of specific humidity and temperature. Similarly, soil moisture was not included, as it has a high correlation with precipitations over a large part of the domain.

Furthermore, to limit multicollinearity among predictors, the set of variables is refined for each grid cell using variance inflation factors (VIF). A commonly guideline is to maintain VIF values below 5 to avoid multicollinearity issues (Jongh et al., 2015). This criterion is enforced through an iterative procedure in which the variable with the highest VIF is removed until all remaining variables satisfy the threshold.

For each cell of the domain, the dominant driver of the trend is determined by the highest trend contribution (TC). For each meteorological variables i, TC_i is determined by:

$$TC_i = \alpha_i \times \text{Trend}(i) \quad (11)$$

with Trend(i) the interannual trend of the meteorological variables (with a significant trend).

Overall, the multilinear models manage to reproduce the trends estimated by CHIMERE with average errors between 13% and 21%.

2.4 Simulation configuration

Simulations are performed over the 1990-2022 period in order to evaluate weather-driven trends taking into account the change in meteorological variables. These simulations are performed using the MEGAN 3.2 emission factors, which are the most up to date and provide the best performance (see evaluation in Section S2.2 in Supplementary Materials).

Several assumptions are made to isolate the effect of meteorological changes from the effect of regulation of other atmospheric anthropogenic pollutants (NMVOC, NOx, NH_3, SOx, PM). The boundary conditions for the entire period are assumed constant and taken from climatology data from GOCART for dust and from the global model LMDZ-INCA for gases and other aerosol species (Mailler et al., 2017). It should be noted that in this setup, as boundary conditions are constant, the evolution

https://doi.org/10.5194/egusphere-2026-4644
Preprint. Discussion started: 9 September 2026

of CH_4 concentrations during the period is not accounted for. The calculated trends therefore isolate the effect of meteorology and cannot be considered as the full effect of climate change as increases of CH_4 global emissions are known to have a strong impact on O_3 concentrations (van Caspel et al., 2024).

Weather conditions such as temperature, precipitation, and wind speed influence the characteristics of fires both in real time but also on the state of vegetation (fuel availability and dryness) notably by the occurrence of droughts (Guion et al., 2022). Due to climate change, Venäläinen et al. (2014b) found an increasing trend in fire meteorological risks for the period 1980–2012 for southern and eastern Europe. However, observational trends in Mediterranean wildfire activity have been negative over the past decades, with a decrease of 66% in annual area burned during the period 1985–2011 (Turco et al., 2016). This is mainly due to improvements in fire management and prevention but also to real-time firefighting. Additionally, Carnicer et al. (2022) analyzed CO_2 emissions from wildfires estimated by the Global Fire Assimilation System version 1.2 (GFASv1.2, based on fire radiative power observations from MODIS instruments) over Europe between 2000 and 2020. Although the authors estimated a statistically significant increase in the Fire Weather Index (which represents the fire risk depending on weather conditions such as fuel moisture and wind speed) over southern and central Europe, they reported no statistically significant trends on the satellite-derived emissions. Due to the lack of data on forest fire emissions taking only the effect of meteorology and the reported lack of emission trend based on satellite data, forest fire emissions are not taken into account our study.

The interannual trend of LAI illustrated by Fig. 1 is assumed to be dominated by climate change during the simulation period. LAI increased during the last decades with a weather-driven trend around 0.0034 $m^2/m^2/yr$ (corresponding to an increase of 0.32%/yr, p-value$<$0.001). This interannual LAI evolution is due to the combination of climate change (due to the increase in CO_2 concentrations and changes in temperature and precipitation) with land-use changes (deforestation or forest restoration). However, several studies reported that climate change (via both the increase in CO_2 fertilization and the evolution of meteorological variables) is the most important driver of LAI changes over Europe (Wu et al., 2023; Zhu et al., 2016). LAI decreases are observed in some areas, especially in France. This decrease is consistent with the results of Laanaia et al. (2016) who estimated a decrease in LAI for broadleaf forests in France after 1990 due to an increase in periods of soil water stress.

In additions to the simulations over the whole period, some sensitivity simulations are also performed over 3 of the coldest years (1991, 1993 and 1996) and 3 of the warmest years (2018, 2019 and 2022), in order to estimate the importance of:

- meteorologically dependent emissions via simulations with meteorologically independent emissions.
- changes in LAI with simulations using the HiQ-LAI data for 2018.

Simulations performed with the CHIMERE version developed in this study are carried out with the H^2O SOA scheme including SOA formation from monoterpene oxidation by autoxidation (Chrit et al., 2017; Sartelet et al., 2020). Following Couvidat et al. (2018), anthropogenic primary organic aerosols are assumed to be semivolatile.

https://doi.org/10.5194/egusphere-2026-4644
Preprint. Discussion started: 9 September 2026

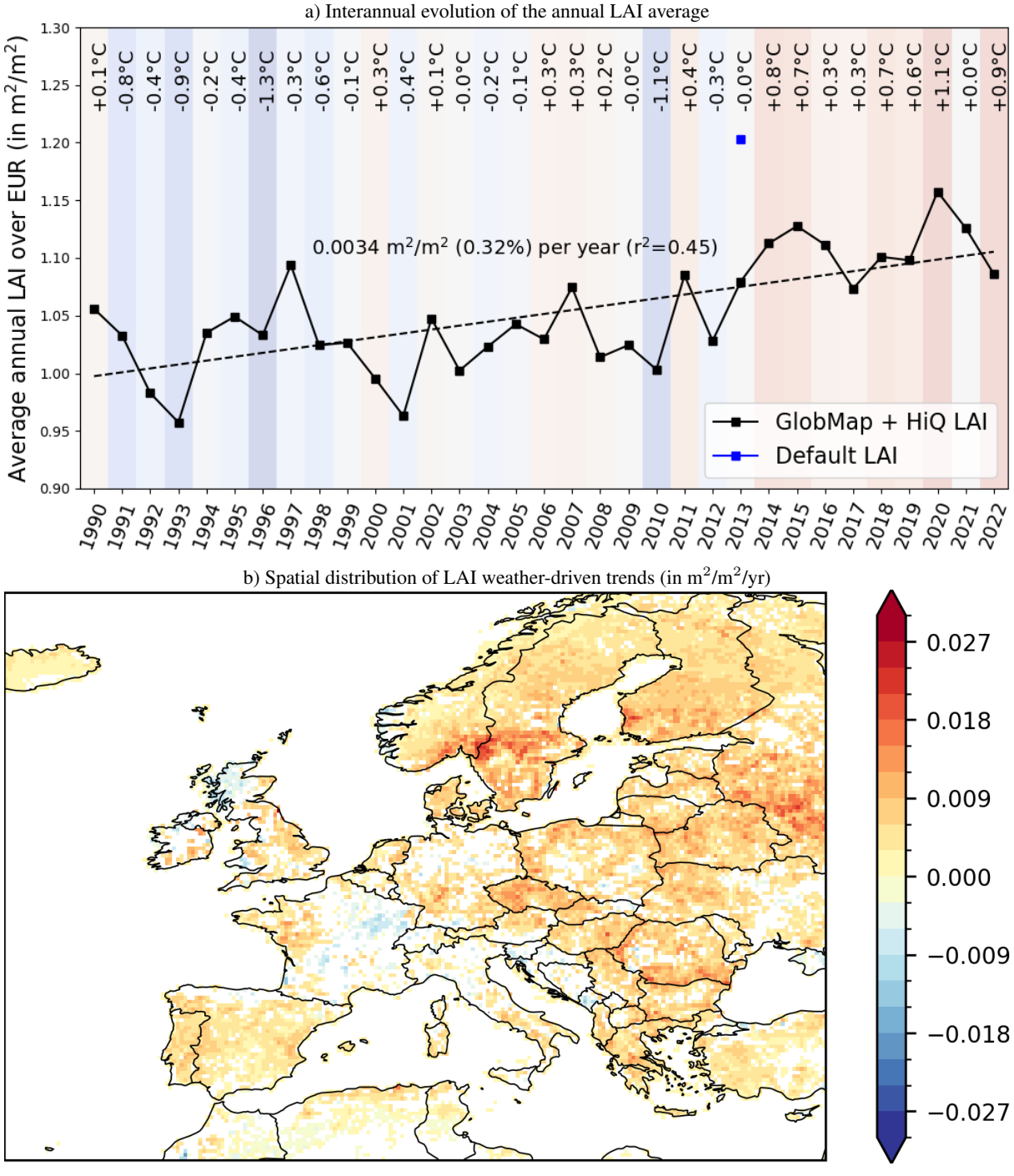

Figure 1. Interannual evolution of the annual LAI average (in m^2/m^2) over EUR (top) and spatial distribution of LAI weather-driven trends (in $m^2/m^2/yr$) (bottom). The bar colors on the background for the graph on the top illustrate variations of the average annual temperature over EUR compared to the average of the 1990-2022 period.

https://doi.org/10.5194/egusphere-2026-4644
Preprint. Discussion started: 9 September 2026

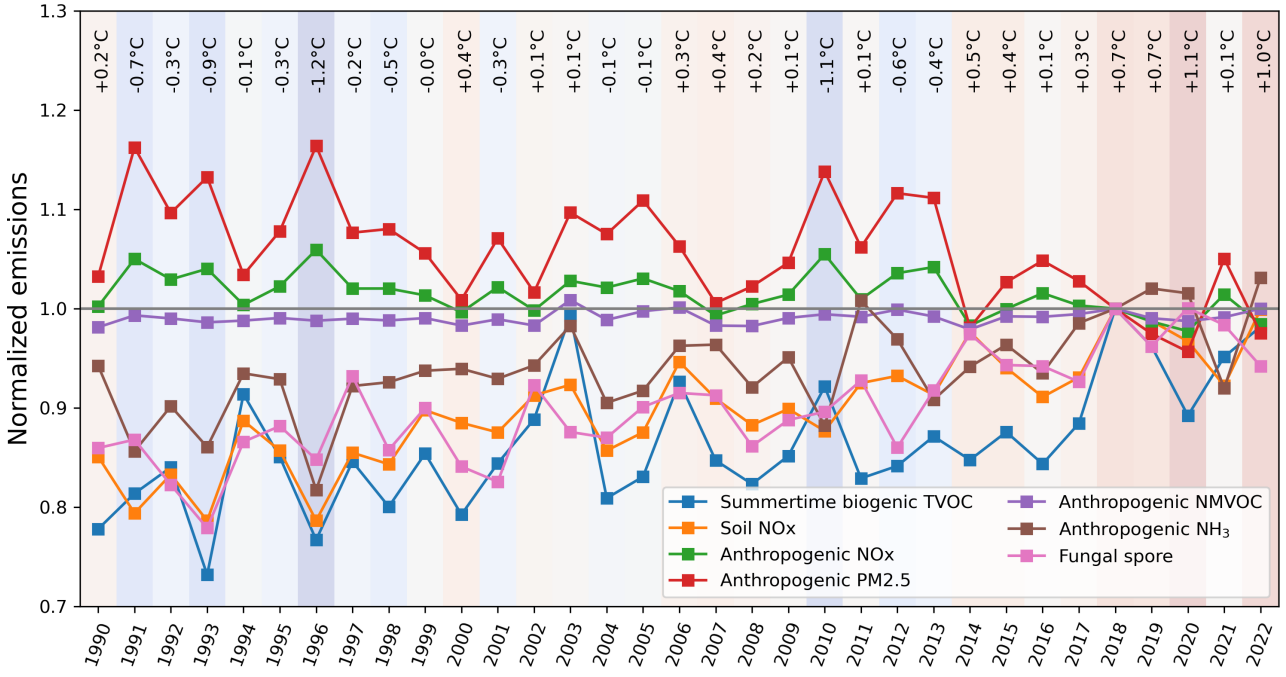

Figure 2. Interannual evolution of all emissions over EUR, normalized relative to 2018 levels. The bar colors on the background illustrate the variations of the average annual temperature over EUR compared the average of the 1990-2022 period.

3 Results and discussions

The determined weather-driven trends on emissions, atmospheric concentrations and deposition over Europe are presented in sections 3.1, 3.2 and 3.3, respectively.

3.1 Weather-driven evolution of emissions

The evolution of emissions over EUR are analyzed by calculating a linear regression between the emissions and either the annual temperatures averaged over EUR (temperature sensitivity expressed in kT/°C) or years (weather-driven trends expressed in kT/yr). Table 1 gives the weather-driven trends and temperature sensitivities of emissions averaged over EUR. Maps of weather-driven trends are shown in Fig. S17 in supplementary materials. As biogenic TVOC are mainly emitted during summer, trends and temperature sensitivities were computed for summer conditions.

In general, due to the temperature dependence taken into account in this study, the determination coefficients (R^2) are higher for temperature sensitivities ($0.50 \leq R^2 \leq 0.93$) than for weather-driven trends ($0.24 \leq R^2 \leq 0.70$). All temperature sensitivities and weather-driven trends averaged presented in Table 1 are statistically significant as all p-values are below 0.01. However, weather-driven trends can be locally statistically nonsignificant due to high p-value (above 0.1). The interannual evolution of emissions over EUR for all emitted compounds is illustrated in Fig. 2.

https://doi.org/10.5194/egusphere-2026-4644
Preprint. Discussion started: 9 September 2026

	Temperature sensitivities		Weather-driven trends	
	Value	R^2	Value	R^2
Summertime biogenic VOC emissions computed with GlobMap+HiQLAI				
Isoprene	121 kT (8.5%) per °C	0.52	4.1 kT (0.29%) per year	0.16
Isoprene (no SM effect)	308 kT (13.8%) per °C	0.77	13.1 kT (0.59%) per year	0.37
Monoterpene	351 kT (15.0%) per °C	0.83	17.4 kT (0.75%) per year	0.53
Sesquiterpene	35.3 kT (21.8%) per °C	0.88	1.89 kT (1.2%) per year	0.66
Others	359 kT (14.4%) per °C	0.83	18.9 kT (0.76%) per year	0.61
TVOC	892 kT (14.0%) per °C	0.83	44.9 kT (0.70%) per year	0.55
Summertime biogenic VOC emissions computed with the default LAI for 2018				
TVOC	862 kT (11.9%) per °C	0.93	36.1 kT (0.50%) per year	0.42
Annual fungal spore emissions				
Default LAI for 2018	24 kT (3.7%) per °C	0.55	1.45 kT (0.22%) per year	0.61
GlobMap + HiQLAI	43 kT (7.7%) per °C	0.50	2.86 kT (0.51%) per year	0.65
Annual NH_3 emissions				
Livestock	87 kT (4.8%) per °C	0.57	3.6 kT (0.20%) per year	0.29
Fertilization application	161 kT (11.0%) per °C	0.72	5.8 kT (0.38%) per year	0.37
Total	248 kT (7.4%) per °C	0.74	9.4 kT (0.28%) per year	0.32
Annual soil NOx emissions (in kT NO_2 eq)				
Natural contribution	60 kT (8.8%) per °C	0.63	3.52 kT (0.51%) per year	0.69
Fertilizer application	49 kT (9.9%) per °C	0.63	2.87 kT (0.58%) per year	0.69
Total	110 kT (9.3%) per °C	0.64	6.40 kT (0.54%) per year	0.70
Annual PM2.5 anthropogenic emissions				
Residential sector	-147 kT (-8.7%) per °C	0.86	-5.52 kT (-0.50%) per year	0.36
Total	-147 kT (-13.3%) per °C	0.86	-5.52 kT (-0.37%) per year	0.36
Annual NOx anthropogenic emissions				
Residential sector	-95 kT (-13.9%) per °C	0.87	-3.4 kT (-0.49%) per year	0.33
Road traffic	-184 kT (-4.8%) per °C	0.84	-5.7 kT (-0.15%) per year	0.24
Total	-279 kT (-3.4%) per °C	0.85	-9.1 kT (-0.11%) per year	0.27
Annual NMVOC emissions anthropogenic emissions				
Residential sector	-145 kT (-13.4%) per °C	0.86	-5.49 kT (-0.50%) per year	0.37
Solvent use	133 kT (5.1%) per °C	0.85	6.06 kT (0.23%) per year	0.53
Gasoline evaporation	7.5 kT (4.7%) per °C	0.79	0.37 kT (0.23%) per year	0.59
Total	-4.7 kT (-0.06%) per °C	0.0	0.94 kT (0.01%) per year	0.04

Table 1. Temperature sensitivities (in kT/textdegree C) and weather-driven trends (in kT/yr) of emissions over EUR between 1990 and 2022. Relative temperature sensitivities and weather-driven trends are provided under parenthesis. R^2: square of the correlation coefficient.

https://doi.org/10.5194/egusphere-2026-4644
Preprint. Discussion started: 9 September 2026

3.1.1 Biogenic VOC and fungal spore emissions

The interannual evolution over EUR of TVOC and isoprene emissions is illustrated by Fig. 3. A significant weather-driven increase in TVOC biogenic emissions over EUR is simulated as they increase by 13.5% per °C (0.67% per year) with a strong correlation to temperature (R^2=0.82). Only a small part of this trend over EUR can be attributed to the interannual evolution of LAI as a similar temperature sensitivity is obtained using the default LAI for 2018 (11.8% per °C).

Although the emissions of all VOCs increase with temperature, the magnitude of this increase varies significantly between specific VOCs. The increase is significantly lower for isoprene (7.9% per °C; 0.31% per year) and higher for sesquiterpene (21.4% per °C; 1.1% per year), which contribute more significantly to SOA formation. The lower increase for isoprene is due to the effect of dry soil conditions that inhibits isoprene emissions when soil humidity is below the wilting point. As illustrated by Fig. 3a, the number of days during summer when soil humidity is below the wilting point increased during the period with a trend of 0.1 days/year (R^2=0.37) from 18.1 days during 1990s to 20.4 during the 2010s. Without this effect, the temperature sensitivity would increase to 14.0% per °C.

Our results are consistent with those of Wang et al. (2024a), who used MEGAN 3.2 to estimate global trends in biogenic emissions over 2000–2020 based on a similar approach, relying on MERRA-2 meteorological data (Gelaro et al., 2017) and time-varying LAI from Yuan et al. (2011). They report an increase in monoterpene emissions over Europe (around 0.8%/yr), in close agreement with our estimate for Europe (0.81%/yr). For isoprene, they obtain a slightly higher trend (0.55%/yr) compared to our estimate (0.43%/yr). Using MEGANv2.1 coupled with the MOHYCAN canopy model, Bauwens et al. (2018) reported an European isoprene trend over 1979–2014 of 0.76%/yr (including the inhibition by CO_2 concentrations) but without considering the effect of soil moisture. This value is slightly higher than our estimate without the effect soil moisture effect (0.66%/yr).

Fungal spore emissions over EUR (illustrated by Fig. 4) are estimated to increase by 0.51% per year (R^2=0.65) and have a better correlation with years than with temperature (R^2=0.50). However, when using the default LAI for 2018 for the entire period, a better correlation coefficient is obtained with temperature (R^2=0.61) than with years (R^2=0.55). The weather-driven trend is then reduced to 0.22% per year, showing that a large part of the trend is driven by the increase in the LAI over EUR. Around 60% of the increase can be attributed to the increase in LAI, the remaining contribution is due to the increase in specific humidity during the same period.

The spatial patterns of weather-driven trends (illustrated by Fig. S15) indicate stronger increases over the eastern half of the domain for both biogenic VOC and fungal spore emissions, reflecting larger increases in temperature and LAI in this region. In contrast, weather-driven decrease in fungal spore emissions are simulated over part of France, associated with decreasing LAI.

3.1.2 Soil NOx emissions

Soil NOx emissions over EUR are estimated to increase by 0.54% per year (R^2=0.70) corresponding to a temperature sensitivity of 9.3% per °C with a similar determination coefficient (R^2=0.64). Fertilizer applications (representing 44% of soil NOx emissions in 2018) and the natural contribution have similar weather-driven trends (0.58% per year and 0.51% per year,

https://doi.org/10.5194/egusphere-2026-4644
Preprint. Discussion started: 9 September 2026

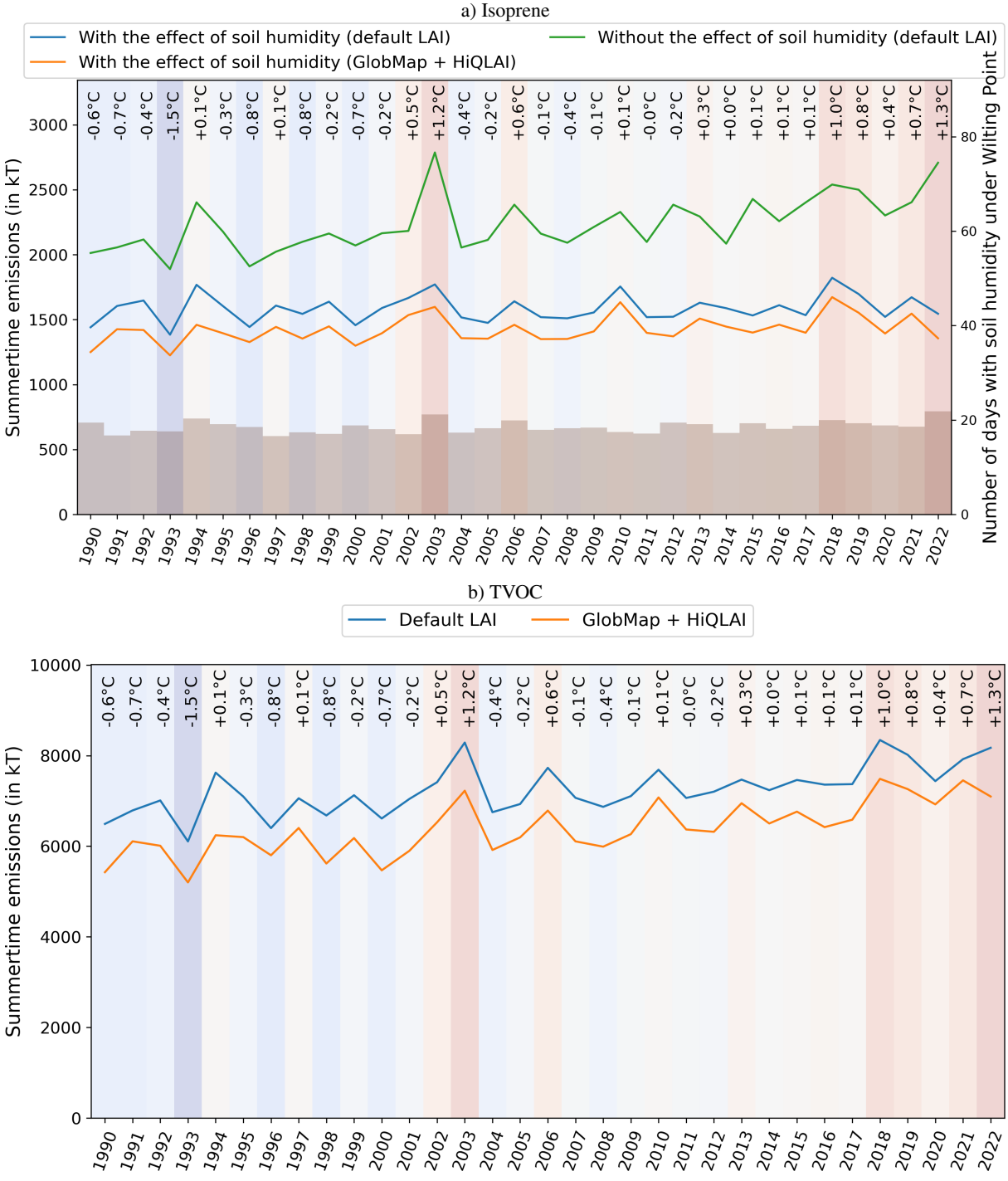

Figure 3. interannual evolution of summertime isoprene (top) and TVOC (bottom) biogenic emissions over EUR. The bar colors on the background illustrate the variations of the average summertime temperature over EUR compared the average of the 1990-2022 period. The brown bar indicates the average number of days where soil humidity is below the wilting point.

https://doi.org/10.5194/egusphere-2026-4644
Preprint. Discussion started: 9 September 2026

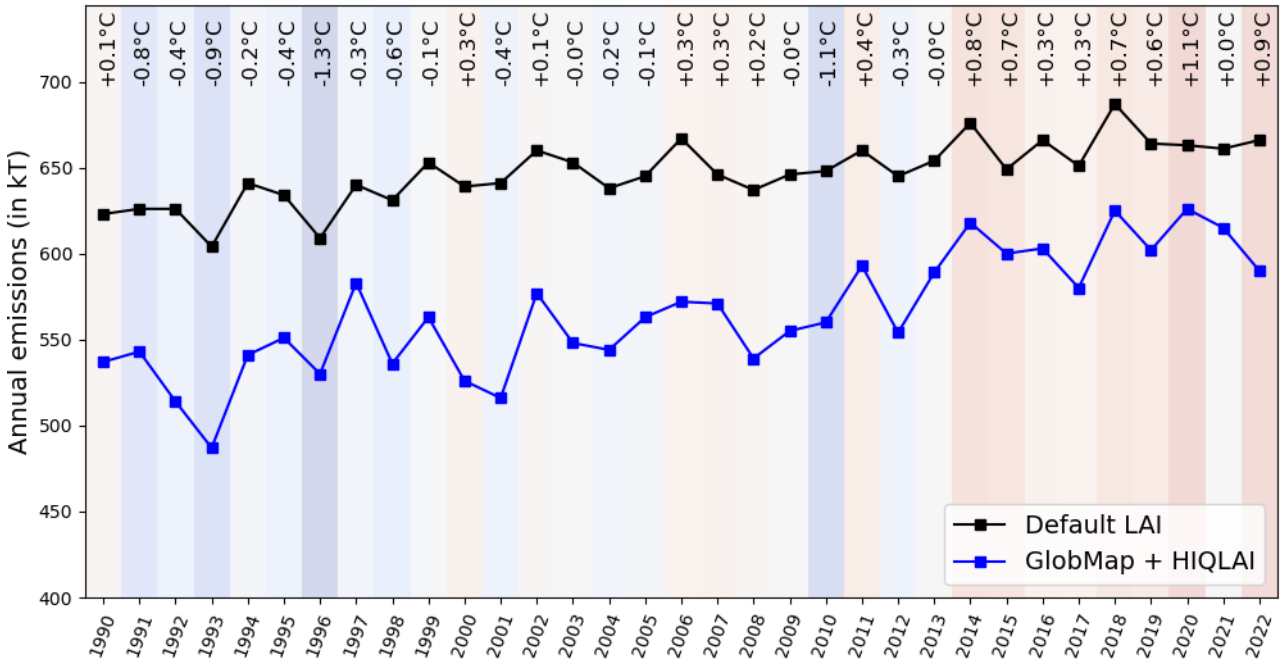

Figure 4. Interannual evolution of fungal spore emissions over EUR. The bar colors on the background illustrate the variations of the average annual temperature over EUR compared the average of the 1990-2022 period.

respectively). Emissions increase across almost the entire domain, with the exception of a few regions with nonsignificant weather-driven trends (especially in Ireland, due to a nonsignificant trend for temperature). The increases in emissions are larger for areas with intensive agricultural activities.

3.1.3 NH_3 emissions from agriculture

NH_3 emissions from agriculture in EUR show a much stronger correlation with annual temperature (R^2=0.74) than with years (R^2=0.32). The emissions are found to increase by 7.4% per °C (0.28% per year). This result is consistent with the increase at the global scale reported by Sutton et al. (2013) (increase in emissions by 8.7% per °C) but higher than the results reported by Jiang et al. (2026) (increase in emissions by 3.8% per °C).

Emissions from livestock (including emissions from manure storage and animal housing and grazing) and from fertilizer applications are both strongly correlated with temperature (R^2 equal to 0.57 and 0.72, respectively) but temperature sensitivities are much higher for fertilizer applications (11.0 % per °C vs. 4.8% for livestock emissions). This behavior is due to the high contribution (85%) of manure storage and animal housing to livestock emissions, which depend (according to the used parameterization) on the temperature inside animal houses or at the surface of the stored manure rather than the outdoor temperature. For example, in houses equipped with forced ventilation, the indoor temperature is assumed to reach a lower limit of 18 °C when the outdoor temperature falls below 12.5 °C, according to the parameterization of Skjøth et al. (2011).

https://doi.org/10.5194/egusphere-2026-4644
Preprint. Discussion started: 9 September 2026

3.1.4 Other anthropogenic emissions

Assuming, in this analysis, that anthropogenic emissions of all other compounds (NOx, NMVOC and PM) are only influenced by meteorology, they show a strong correlation with temperature ($R^2 \geq 0.79$) while the correlation with years is moderate ($R^2 \leq 0.59$). Only total NMVOC emissions have no significant trends due to compensation between the increase in NMVOC emissions from gasoline evaporation and the use of solvents (resulting in an increase of 140 kT per °C) and the decrease in emissions from the residential sector (-145 kT per °C). Although the weather-driven trend of NMVOC emissions is close to zero, winter emissions decrease with increasing annual temperatures (due to reduced residential emissions) while summer emissions increase (due to increased emissions from solvent use and gasoline evaporation).

Anthropogenic emissions of PM2.5 and NOx are found to decrease with increasing temperatures. PM2.5 emissions are only affected by the decrease in the residential sector emissions, leading to a decrease in total PM2.5 emissions (including all sectors) of -13.3% per °C (-0.37% per year). Total NOx emissions decrease by 3.4 % per °C (-0.11% per year) with approximately two-thirds of the weather-driven trend attributable to reductions in diesel traffic emissions, and the remaining fraction due to the residential sector. Spatially, weather driven trends of NOx and PM2.5 are negative across almost the entire domain. Trends are especially important in region with large anthropogenic emissions (especially in Italy and eastern EUR countries for PM2.5 and in densely urbanized areas for NOx).

CHIMERE also considers emissions of sea salt, mineral dust and urban dusts. However, the European trends of mineral and urban dusts emissions and the trends of sea salt emissions over the whole domain are statistically non-significant. Trends of mineral dust emissions over the African part of the domain are around 380 kT/yr (around 0.39%/yr) but are only slightly statistically significant (p-value equal to 0.077).

3.2 Weather-driven evolution of atmospheric concentrations

The determined dominant drivers and the distribution of significant weather-driven trends in annual concentrations of O_3, NO_2, and PM10 as well in SOMO35, and total deposition over EUR of oxidized sulfur ($S_{oxidized}$), reduced nitrogen ($N_{reduced}$), and oxidized nitrogen ($N_{oxidized}$) are illustrated by Fig. 5. The interannual evolution of population-weighted concentrations and deposition as well as the population-weighted weather-driven trends and temperature sensitivities are also shown in supplementary materials (Fig. S18 and Table S1).

3.2.1 Ozone concentrations

The weather-driven evolution of several O_3 metrics typically used in air quality are investigated: annual mean concentrations, the annual average of daily maxima, the sum of ozone daily 8-h maximum over 35 ppb (SOMO35), the accumulated ozone exposure over a threshold of 40 ppb for vegetation and crops (AOT40c) and the fourth daily maximum 8-hour average (4MDA8).

Annual mean concentrations, the annual average of daily maxima, SOMO35 and AOT40c exhibit moderate correlations with temperature (R^2 = 0.37, 0.43, 0.38 and 0.26, respectively), whereas correlations with time are weak (R^2 = 0.10-0.18). Consequently, the inferred population-weighted trends are only moderately significant for the annual average of daily maxima

https://doi.org/10.5194/egusphere-2026-4644
Preprint. Discussion started: 9 September 2026

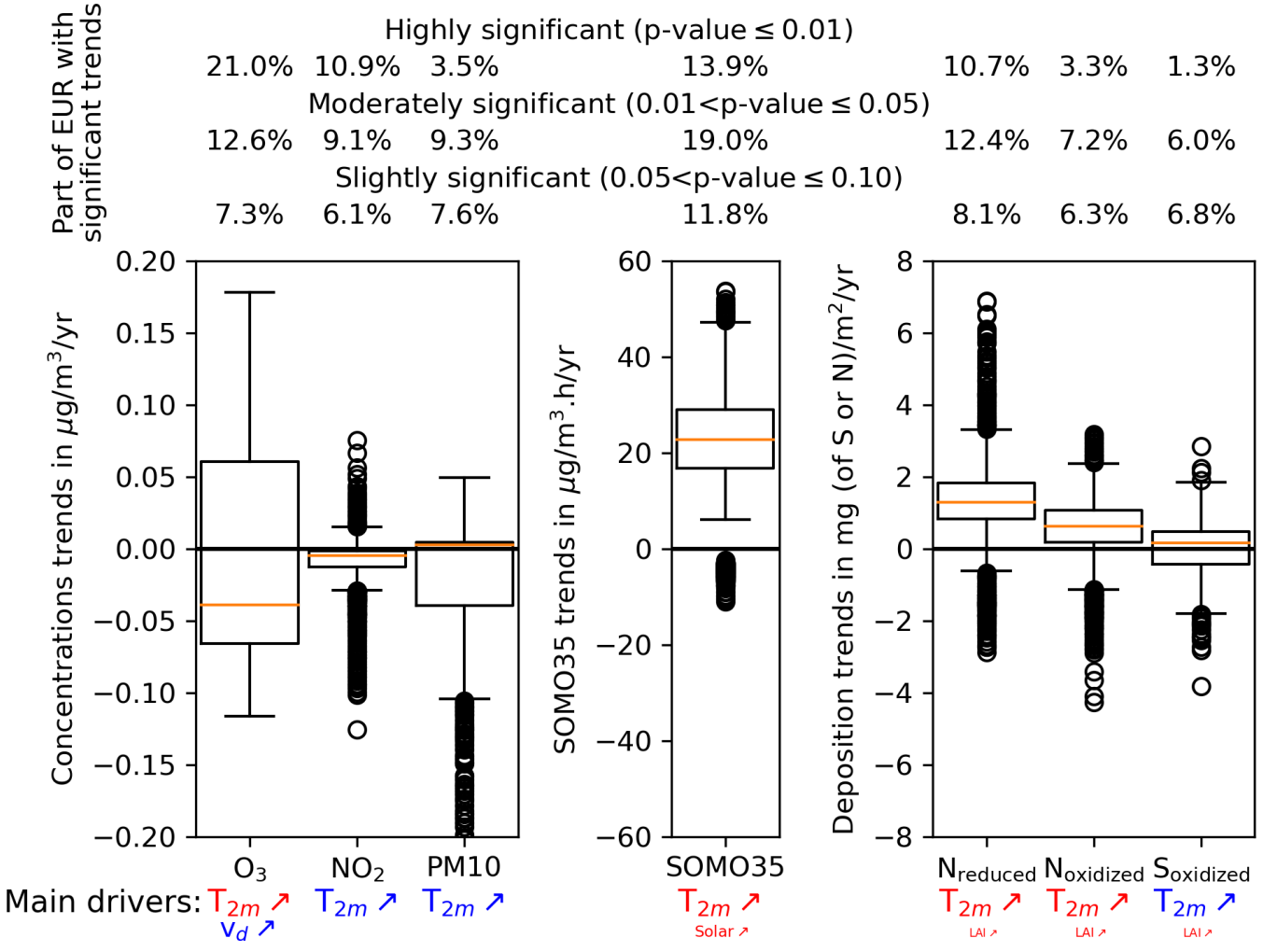

Figure 5. Box plots of statistically significant weather-driven trends (1990-2022) in annual concentrations of O_3, NO_2, and PM10 as well in SOMO35 and total deposition over EUR of oxidized sulfur (Soxidized), reduced nitrogen ($N_{reduced}$), and oxidized nitrogen ($N_{oxidized}$). The fraction of EUR exhibiting statistically significant trends is indicated at the top of the figure. The dominant drivers of these trends are shown at the bottom, with symbol sizes weighted by their relative importance. Drivers shown in red and blue correspond to positive and negative trends, respectively.

https://doi.org/10.5194/egusphere-2026-4644
Preprint. Discussion started: 9 September 2026

(p-value = 0.029), SOMO35 (p-value=0.013), AOT40c (p-value=0.028) and weakly significant for the annual mean (p-value = 0.070). In contrast, population-weighted ozone 4MDA8 shows a low correlation with annual temperature (R^2 = 0.14), indicating that, unlike the other metrics, its temporal evolution cannot be explained by changes in mean annual temperature. This result is expected, as 4MDA8 is representative of ozone daily peaks and is therefore associated with extreme conditions that are not necessarily correlated with annual mean temperature. Accordingly, weather-driven trends in population-weighted 4MDA8 are not statistically significant (p-value = 0.23), reflecting the sporadic occurrence of years with elevated 4MDA8 values (e.g., 1994, 2003, 2006, and 2019). The weather-driven trends are particularly strong for SOMO35 and AOT40c with population-weighted trends of 0.5%/yr and 0.69%/yr (corresponding to overall increases by 18% and 22% over the 1990–2022 period), respectively. A population weighted trend of 0.07%/yr is found for O_3 annual concentrations.

The spatial distributions of R^2 for annual O_3 and SOMO35 are shown in Fig. 6. Determination coefficients (R^2) with temperature are highest over Spain and Southwestern France indicating that temperature is probably an important meteorological driver of annual O_3 concentrations over this region. Determination coefficients with temperature remains low in the other regions. Similar spatial distribution are found for SOMO35, except that R^2 are close to 0 in Northern Europe and higher in Eastern Europe. Very high R^2 (around 0.5-0.6) with temperature are found for AOT40c over almost the domain (with the exception of Scandinavia), indicating a very high relationship of AOT40c with annual temperatures. 4MDA8 has a very different pattern with low interannual R^2 values over the whole domain but they can reach 0.4 locally.

Fig. 7 shows the maps of weather-driven trends calculated over the domain for O_3 annual means and SOMO35. Maps for the annual averages of daily maximums, 4MDA8 and AOT40c are also shown in the supplementary materials. Given the lack of significance of weather-driven trends for 4MDA8 and the similarity of patterns between annual O_3 concentrations and annual average and between SOMO35 of AOT40c, the discussion of weather-driven trends is limited to annual mean O_3 and SOMO35.

Weather-driven trends for annual ozone concentrations are found to be statistically significant (p-value < 0.1) over two areas of the European domain: southern Europe around the Mediterranean sea (especially in Spain and Southeastern France) with positive trends (exceeding 0.15 $\mu g/m^3$/yr in the Rhône valley in Southeastern France) and northern Europe with negative trends (between -0.05 $\mu g/m^3$/yr and -0.12 $\mu g/m^3$/yr over a larger part of Scandinavia). In contrast, significant trends for SOMO35 were found to be always positive. Statistically significant trends are found over most of Europe with the exception of Italy and a large part of Northern Europe (including the united kingdom, Ireland, Scandinavia, the baltic countries and Russia). Trends are generally between 20 and 60 $\mu g/m^3$.h/yr.

Although R^2 coefficients with temperature and years are weak, the multilinear regression using meteorological drivers yields R^2 values exceeding 0.7 for both annual mean O_3 and SOMO35 over most of Europe. The dominant meteorological drivers of trends in annual mean O_3 concentrations and SOMO35 are shown in Fig. 8. Two main geographical regimes can be identified for annual mean O_3 concentrations. First, Northern Europe exhibits significantly negative weather-driven trends, primarily driven by increases in deposition velocities. Second, Southern Europe is characterized by positive trends, largely attributable to increases in T_{2m}. Additional drivers can be locally dominant, including decreases in the deposition velocity (notably over Eastern France), increases in solar radiations , and increases in PBL, which enhance vertical mixing and promote the import of O_3 from the upper layers. Concerning SOMO35, two main drivers were identified: the increase in T_{2m} (dominant driver over

https://doi.org/10.5194/egusphere-2026-4644
Preprint. Discussion started: 9 September 2026

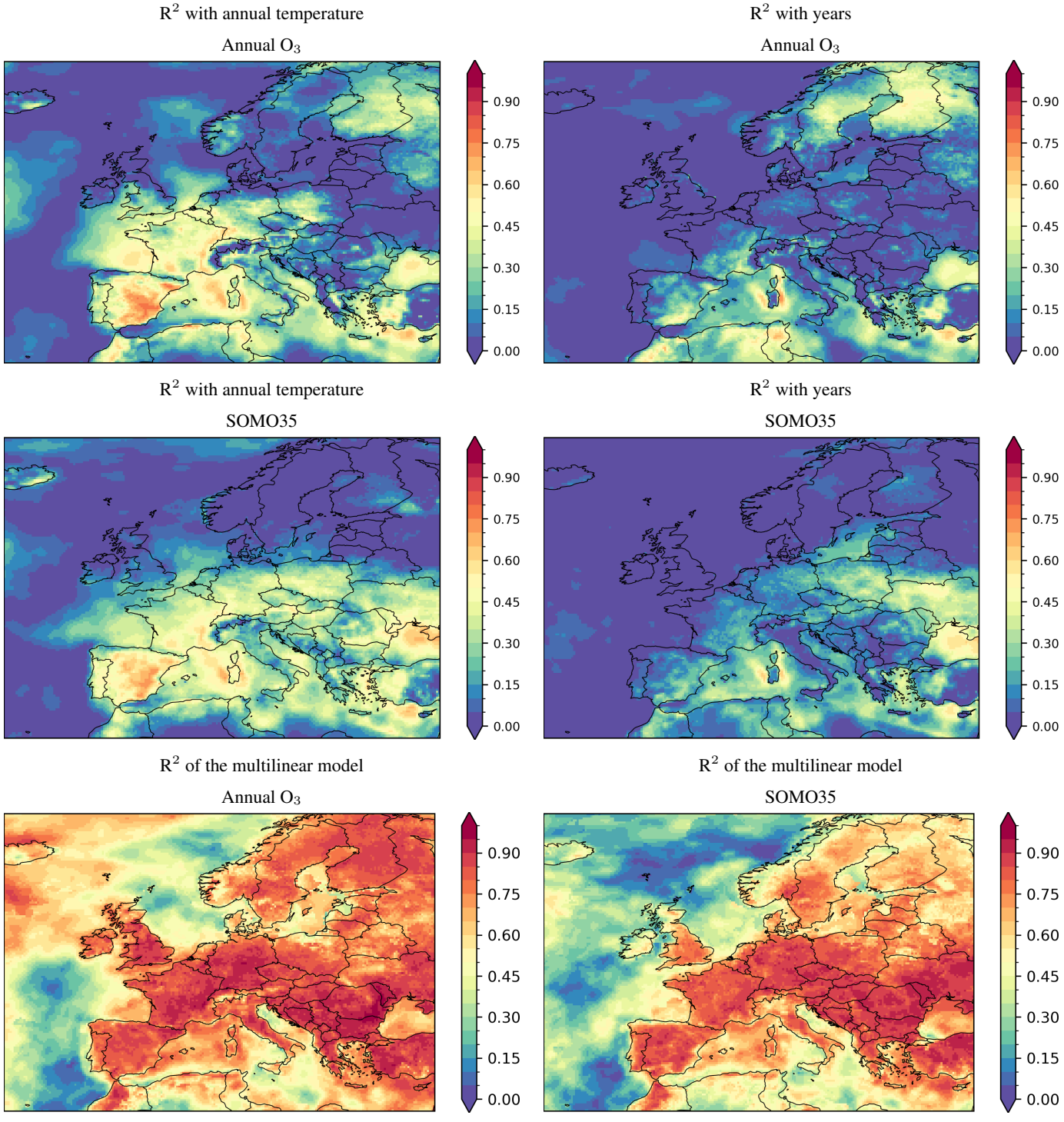

Figure 6. Determination coefficient with annual temperature, years and of the multilinear model for O_3 annual concentrations and SOMO35.

https://doi.org/10.5194/egusphere-2026-4644
Preprint. Discussion started: 9 September 2026

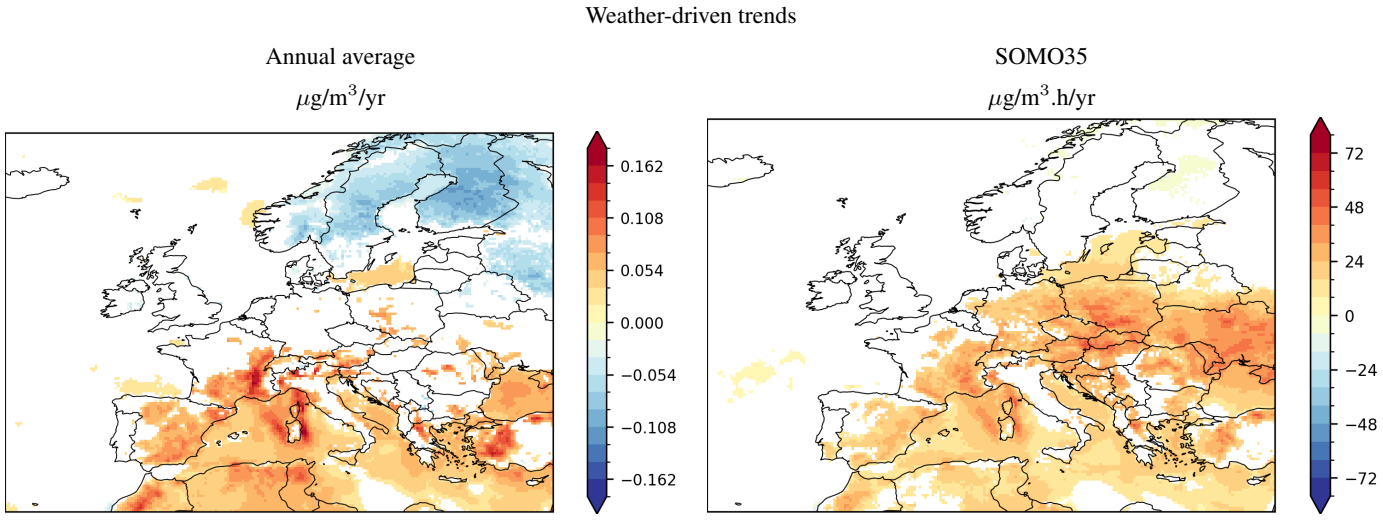

Figure 7. Maps of statistically significant weather-driven trends between 1990 and 2022 over Europe for the annual ozone concentrations and SOMO35. Only areas with a slight significant trend (p-value<0.1) are shown.

most of the domain with significant trend) and the increase in solar radiation (can be dominant over part of Germany, Poland and Ukraine). Other drivers can contribute such as changes in LAI and deposition velocities.

Otero et al. (2018) indicated that one major driver of O_3 concentration interannual variability is relative humidity and that CTMs had trouble representing the dependence to this driver. The authors postulate that the dependence to this driver may be related to dry-deposition schemes in the air-quality models that may miss a link between humidity and stomatal uptake. We find that deposition velocity is both the main driver for weather-drivern trends and for the interannual variability. Without using deposition velocities as a driver in the multilinear model, RH is an important driver of the variability together with solar radiations and temperature, consistently with the results of Otero et al. (2018).

Changes in the deposition velocities of O_3 between the selected hot and cold years over Europe are illustrated in Fig. 9. A large part of northern and eastern Europe is characterized by an increase in deposition velocities when the interannual LAI evolution is taken into account consistently with the positive weather-driven trend of LAI illustrated by Fig. 1b. In contrast, large parts of western and central Europe are associated with a decrease in deposition velocities driven by an increase in the number of days above the optimal temperature for deposition (around 20°C for forests, Emberson et al. (2000)). The combination of the evolution of O_3 concentrations and deposition velocities leads to an overall increase in ozone dry deposition, although local decreases are simulated.

The decrease in ozone metrics over Northern Europe can be explained by the increase in LAI over this region, leading to an increase in deposition velocities. Based on the sensitivity simulations conducted for the selected cold and hot years (the difference hereinafter referred to as "Diff$_{H-C}$"), using a constant LAI would lead to an increase of Diff$_{H-C}$ in Finland for O_3 annual concentrations of 1.06 μg/m^3. LAI increased in Finland by 0.153 m^2/m^2 (18%) between the hot and cold years, leading to an increase in deposition velocities of 0.036 cm/s (12.5%) instead of only 0.014 cm/s when LAI is held constant.

https://doi.org/10.5194/egusphere-2026-4644
Preprint. Discussion started: 9 September 2026

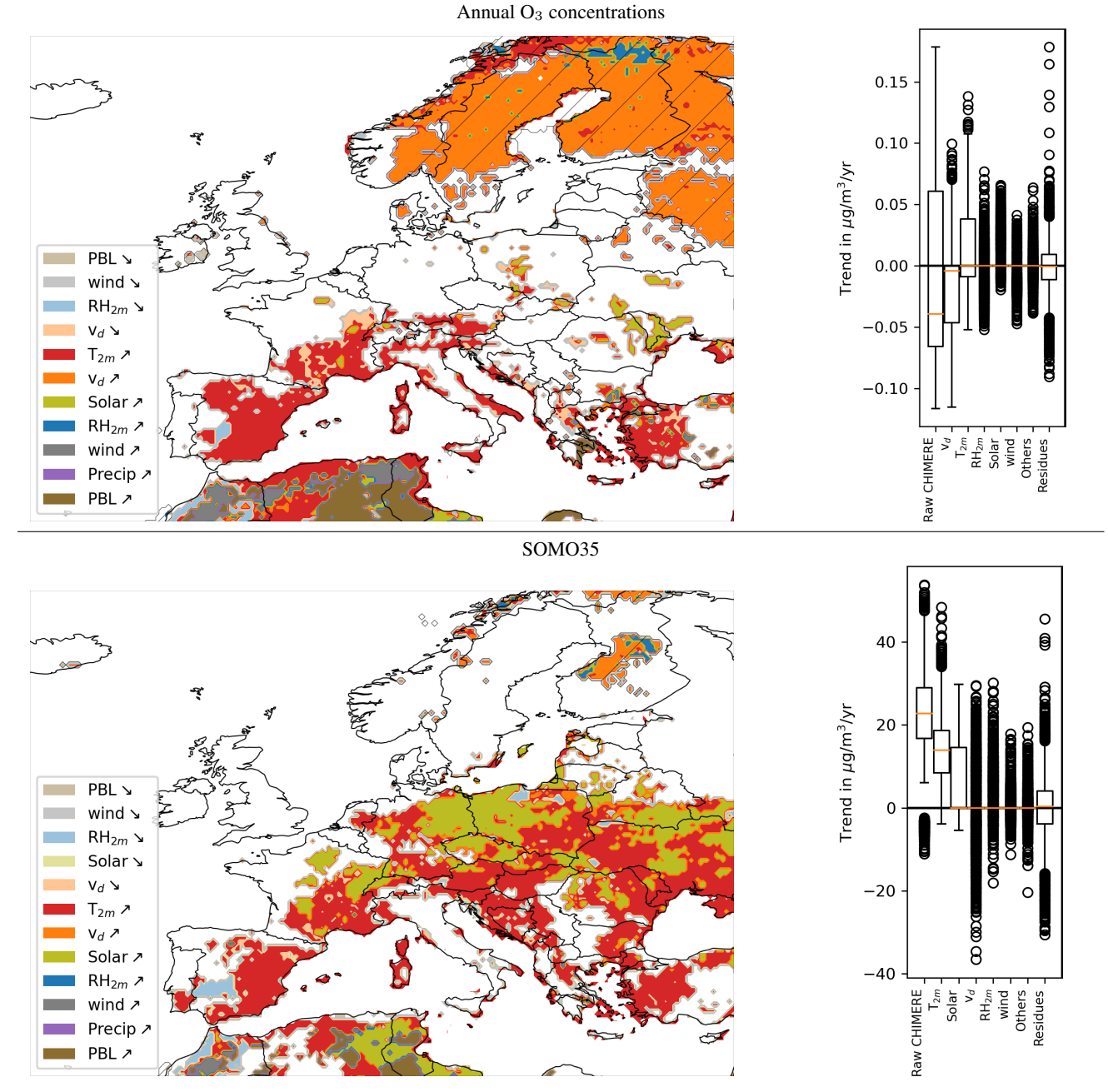

Figure 8. Map of the dominant meteorological driver (left) and box plot of the estimated contribution over EUR of each driver (right) for O_3 annual concentrations (top) and SOMO35 (bottom). The annual average are used for the O_3 annual concentrations. Only cells with significant weather driven trends are shown. Only the first 5 five dominant drivers in the boxplot, the sum of the contributions of the other drivers are shown in "Others". "Residues" represent the difference between the trend calculated with CHIMERE results and the sum of contributions of all meteorological drivers.

https://doi.org/10.5194/egusphere-2026-4644
Preprint. Discussion started: 9 September 2026

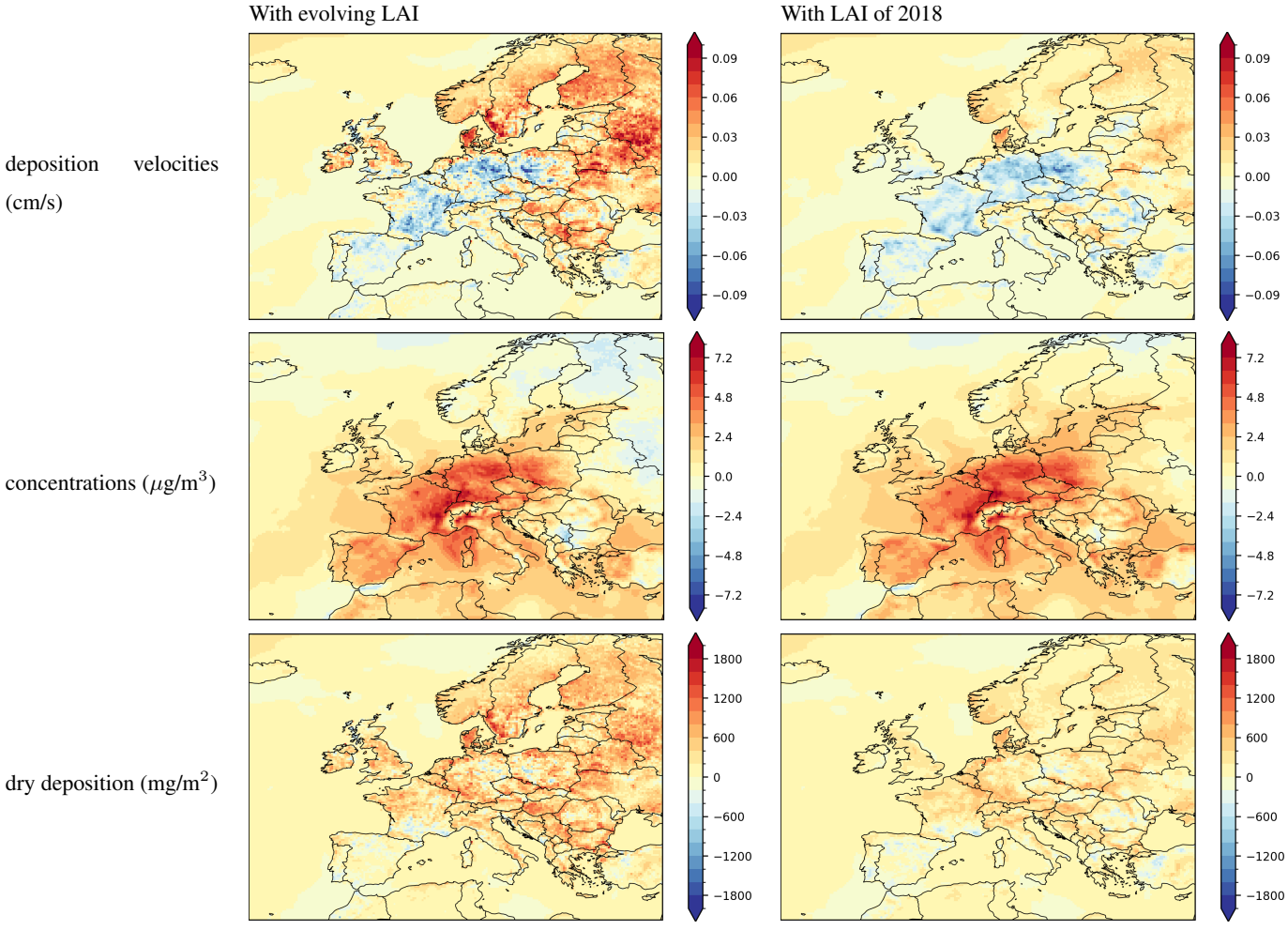

Figure 9. Changes in annual deposition velocity of O_3 (top, in cm/s), annual O_3 concentrations (middle in $\mu g/m^3$) and O_3 dry deposition (bottom in mg/m^2) between the selected hot and cold years.

https://doi.org/10.5194/egusphere-2026-4644
Preprint. Discussion started: 9 September 2026

3.2.2 Nitrogen dioxide

The maps of temperature sensitivities and weather-driven trends (as well as the corresponding R^2) for annual concentrations of NO_2 are shown in Fig. 10. The population-weighted weather-driven trends over EUR is only slightly statistically significant (p-value=0.079).

Overall, the coefficients of determination are substantially higher for regressions against temperature (average R^2 over EUR of 0.24) than interannual regressions (average R^2 of 0.08), reflecting the strong sensitivity of NO_2 concentrations to NO_x emissions. The multilinear model successfully reproduces the evolution of annual mean NO_2 concentrations, with R^2 values exceeding 0.6 over large portions of the domain. However, lower performance ($R^2 < 0.5$) is obtained in parts of Northern, Eastern, and Southern Europe. Statistically significant trends are simulated over the Alpine region and across much of Southern Europe and are predominantly negative, except in a few marine areas along major shipping routes. Weather-driven trends are particularly pronounced over the Alps, where they reach values below -0.05 $\mu g/m^3$/yr.

Consistent with the relatively high R^2 values for temperature across most of the domain, the multilinear model identifies temperature as the primary driver, leading to a decrease in NO_2 annual concentrations over nearly the entire region (Figure 11). While other meteorological factors have near-zero median contributions, variables such as solar radiation, wind speed and RH can locally influence NO_2 trends.

The decrease in NO_2 concentrations due to temperature arises from the temperature dependence explicitly accounted for in the model. Indeed, weather-driven trends should be negligible when the temperature dependence of anthropogenic emissions is not taken into account. In that case, the average $Diff_{H-C}$ over Europe for annual NO_2 is around 0.039 $\mu g/m^3$ against -0.206 $\mu g/m^3$ (around -6% of EUR NO_2 annual concentration) when temperature-dependent emissions are used.

3.2.3 Particles

Strong negative population-weighted weather-driven trends are found for PM2.5 and PM10 (-0.030 $\mu g/m^3$/yr and -0.033 $\mu g/m^3$/yr, corresponding to overall decreases over 1990-2022 by 0.95 and 1.04 $\mu g/m^3$, respectively), which are statistically significant (p-value < 0.05). These trends are primarily driven by the evolution of secondary inorganic aerosols (SIA), which exhibit a population-weighted weather-driven trend of -0.016 $\mu g/m^3$/yr (p-value < 0.05), and primary anthropogenic aerosols (PAA), with a population-weighted weather-driven trend of -0.019 $\mu g/m^3$/yr (p-value < 0.01). In contrast, secondary organic aerosols (SOA) and fungal spores show weak positive weather-driven trends across Europe, with population-weighted trends of 0.0016 $\mu g/m^3$/yr and 0.0019 $\mu g/m^3$/yr, respectively (p-value < 0.01). Trends are statistically nonsignificant for other compounds (dusts and sea salts) but dusts have a statistically significant sensitivity to temperature. However, this dependency is likely due to higher dust concentrations during the last years, which are also the hottest years. Simulated dust concentrations are especially high in 2022 due to high dust intrusion into the domain. These results are consistent with those of Cuevas-Agulló et al. (2024) who reported higher winter dust intrusion in western Euro-Mediterranean during the 2020-2022 period compared to the 2003-2019 period.

https://doi.org/10.5194/egusphere-2026-4644
Preprint. Discussion started: 9 September 2026

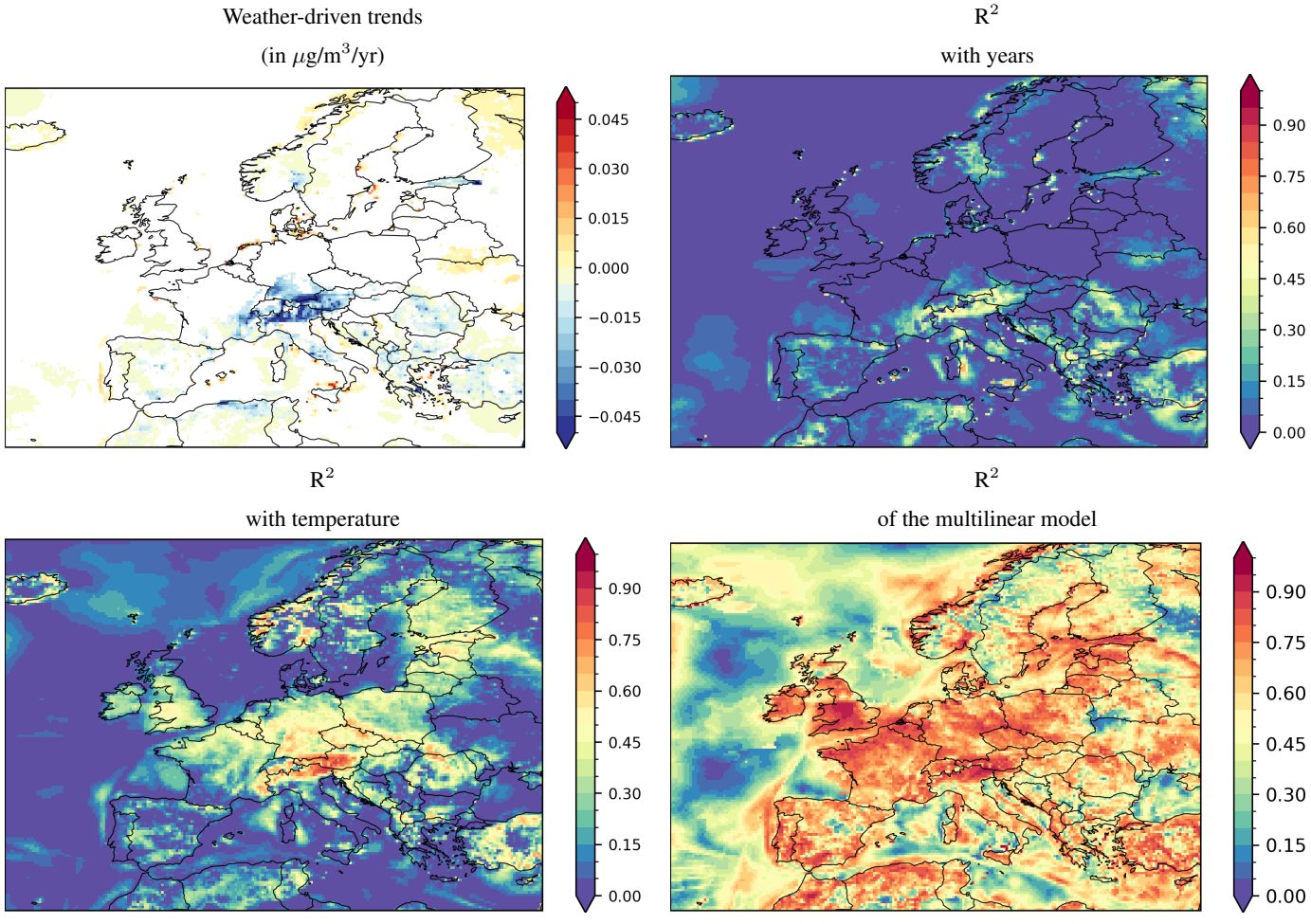

Figure 10. Maps of statistically significant weather-driven trends of NO_2 annual concentrations and R^2 of concentrations with years, temperature and of the multilinear model.

As PM10 and PM2.5 exhibit similar weather-driven trends (with comparable mean R^2 values for the multilinear models: 0.63 for PM10 and 0.61 for PM2.5), the analysis focuses on PM10, which include fungal spore concentrations (> 2.5 μm), unlike PM2.5. Interannual weather-driven trends and the determined dominant meteorological drivers for PM10 annual concentrations are illustrated by Figures 12 and 13. The corresponding maps for PM2.5 are also shown in Supplementary materials (Figures S24 and S25).

PM10 annual concentrations have stronger correlation with temperature (R^2 reaching 0.3-0.5 especially over Northern France, part of Eastern and Northern Europe) than with years (except in Italy, where correlations with years reach 0.3-0.5). The multilinear model reaches R^2 above 0.5 over almost the entire domain (average R^2 over EUR of 0.71). Statistically significant negative trends (exceeding -0.10 μg/m^3/yr in the Po Valley) are simulated in southwestern quarter of Europe, driven primarily

https://doi.org/10.5194/egusphere-2026-4644
Preprint. Discussion started: 9 September 2026

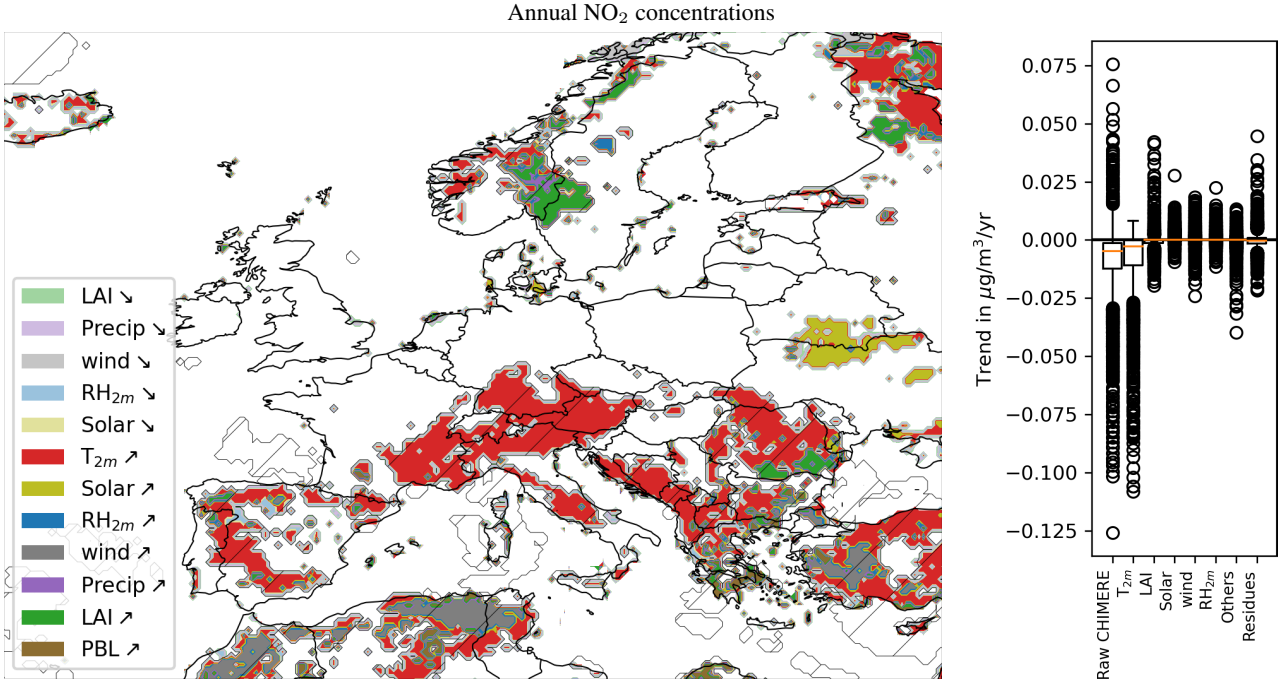

Figure 11. Map of the dominant meteorological driver (left) and box plot of the estimated contribution over EUR of each driver (right) for NO_2 annual concentrations. Only cells with significant weather driven trends are shown. "Residues" represent the difference between the trend calculated with CHIMERE results and the sum of contributions of all meteorological drivers.

by increases in temperature. In contrast, statistically significant negative trends are found in the northern region of the domain due to increases in temperature and LAI. These contrasting effects of temperature on PM10 concentrations arise from opposing responses of specific PM components. Trends in the southwestern Europe are primarily driven by decreases in SIA and total particulate matter (TPM) concentrations, whereas trends in northern Europe are largely due to increases in SOA and fungal spore concentrations.

As illustrated by Fig. S18, while temperature trends explained a large part of PM10 trends, other factors (especially the wind direction and the PBL) explained most of the interannual variability. PBL is the dominant driver of the variability of PM10 concentrations across a large part of Europe (the United Kingdom and Ireland, and a large part of Eastern and Northern Europe). In certain regions, particularly near NH_3 emission hotspots (e.g., Brittany and extensive areas of the Benelux countries and Germany), the average wind velocity originating from these hotspots (from the east or from the west depending on region) also constitutes a major driver.

Using the multilinear approach to isolate the effect of temperature, changes on PM2.5 concentrations due to temperature is generally negative, in particular over central Europe with changes ranging from -2.0 to 0.1 $\mu g/m^3/K$. These changes are much more negative than the results reported by Megaritis et al. (2014) who reported values estimated with PMCAMx-2008 between -0.7 and 0.3 $\mu g/m^3/K$. However, Megaritis et al. (2014) did not consider an effect of temperature on Primary Anthropogenic

https://doi.org/10.5194/egusphere-2026-4644
Preprint. Discussion started: 9 September 2026

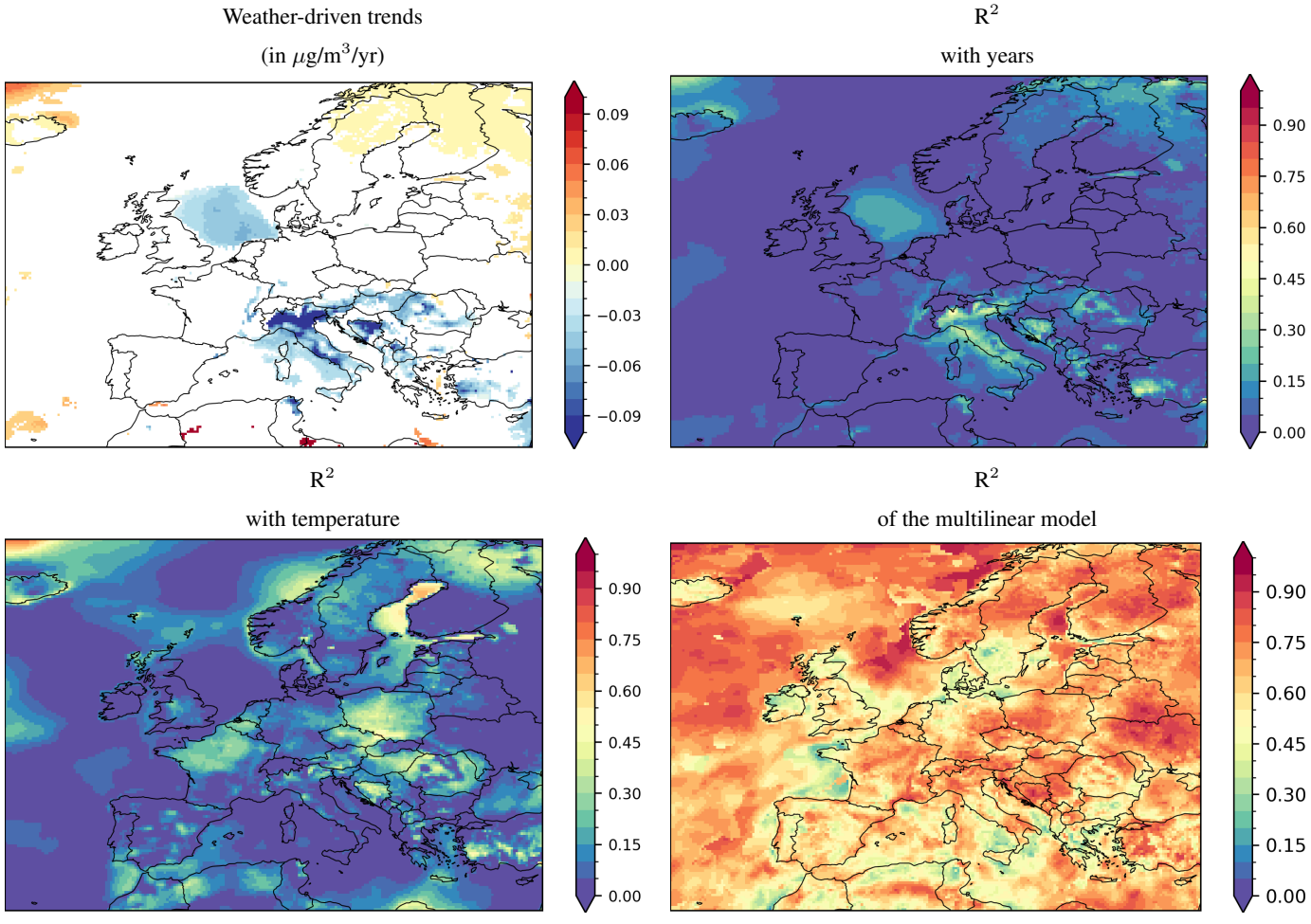

Figure 12. Maps of weather-driven trends of PM10 annual concentrations and R^2 of concentrations with years, temperature and of the multilinear model.

Aerosol (PAA) emissions and mainly observed a decrease of SIA, whereas PAA are the components with the highest decrease in our results.

To better understand PM trends, they are analyzed separately for each major PM component class: PAA, SIA, Primary natural aerosols (PNAT) and SOA. The maps of weather-driven trends, R^2 with years, R^2 of the multilinear model and of the dominant drivers are shown in Supplementary materials (Figures S27 to S31).

https://doi.org/10.5194/egusphere-2026-4644
Preprint. Discussion started: 9 September 2026

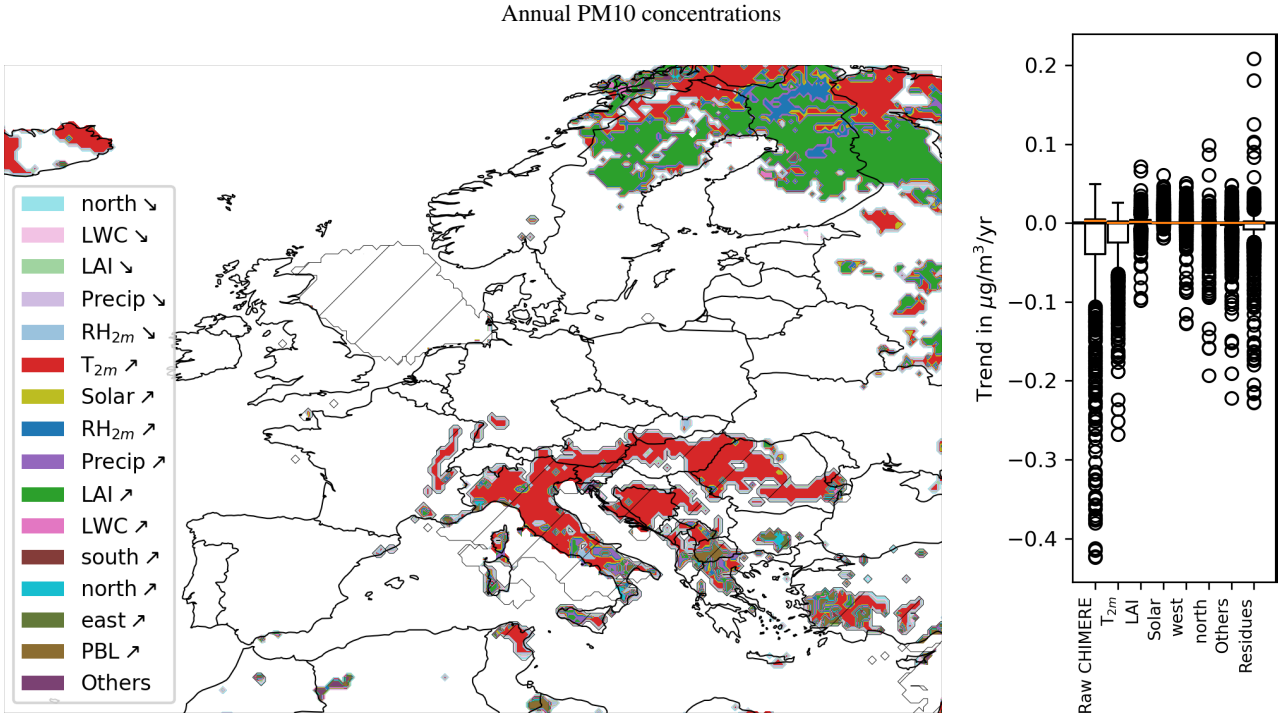

Figure 13. Map of the dominant meteorological driver (left) and box plot of the estimated contribution over EUR of each driver (right) for PM10 annual concentrations. The 14 first dominant drivers (with a positive or negative trend) are shown in the map of the dominant drivers, cells where the evolution of PM10 concentrations is dominated by other drivers are gathered in "Others". Similarly, only the first 5 five dominant drivers in the boxplot, the sum of the contributions of the other drivers are shown in "Others". "Residues" represent the difference between the trend calculated with CHIMERE results and the sum of contributions of all meteorological drivers.

3.2.4 Primary anthropogenic Aerosol

A significant decrease in PAA concentrations due to meteorological changes is simulated over EUR with the most important negative population-weighted weather-driven trends (-0.019 μg/m^3/yr) for PM components. The most important decreases are simulated in Italy (especially in the Po Valley with a trend of -0.10 μg/m^3/yr) and the Balkans.

515 This decrease is primarily driven by the reduction in PM emissions from the residential sector associated with higher annual temperatures. Sensitivity simulations indicate that this concentration decrease is largely attributable to the temperature dependence of emissions: the Diff$_{H-C}$ value rises from -0.419 μg/m^3 to -0.060 μg/m^3 when emissions are assumed to be independent of meteorological conditions. The multilinear model further confirms that the observed trend in PAA concentrations is almost entirely explained by the trend in annual temperatures.

https://doi.org/10.5194/egusphere-2026-4644
Preprint. Discussion started: 9 September 2026

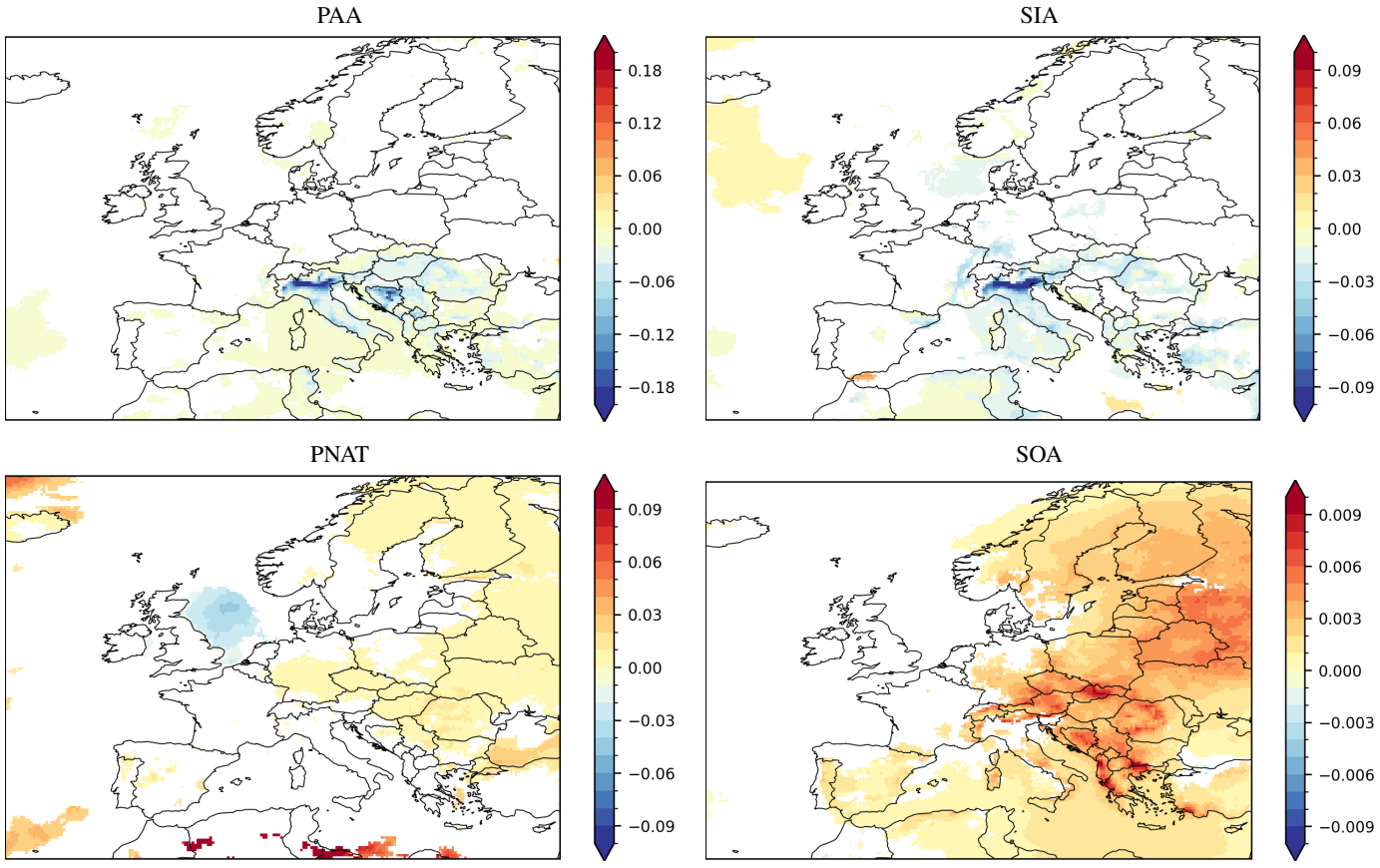

Figure 14. Maps of weather-driven trends (in $\mu g/m^3/yr$) over Europe for PM component concentrations.

3.2.5 Secondary Inorganic Aerosol

SIA is the second PM component with the largest negative trend (population-weighted trend of -0.0155 $\mu g/m^3/yr$). The highest decreases are simulated over the Po Valley where it exceeds 0.10 $\mu g/m^3/yr$. Positive trends are simulated in the region of the Gibraltar Strait (characterized by high marine traffic emissions) where it can exceed 0.03 $\mu g/m^3/yr$. R^2 for weather-driven trends is over 0.1 over a large part of EUR except Northern Europe, Ireland and the United Kingdom. While R^2 with temperature is generally low for southern Europe and northern Europe, R^2 values greater than 0.4 are simulated over Northern France and Poland.

The evolution of SIA is dominated by ammonium nitrate as only 2% of the weather-driven trend can be explained by sulfate (SO_4). The evolution of ammonium nitrate concentrations are controlled by multiple factors: the decrease in NOx emissions from traffic and residential sectors, the increase in NH_3 emissions from agriculture, the increase in NOx emissions from soils, and the reduction in conditions favorable to ammonium nitrate formation (which is promoted by cold and humid conditions). Depending on which factor is limiting, SIA concentrations could theoretically increase or decrease. To assess the relative

https://doi.org/10.5194/egusphere-2026-4644
Preprint. Discussion started: 9 September 2026

importance of these factors, Diff_{H-C} in SIA concentrations was analyzed for the different sensitivity simulations. The mean Diff_{H-C} increases from -0.46 μg/m^3 to -0.30 μg/m^3 when weather-independent emissions are taken into account, suggesting that temperature-driven effects on ammonium nitrate formation are likely the primary driver of the simulated SIA evolution. The multilinear model further confirms that trends in SIA concentrations are strongly dominated by the trend in temperature.

3.2.6 Secondary organic Aerosol

For SOA, a weak positive population-weighted weather-driven trend of 0.0016 μg/m^3/yr is estimated. However, this increase corresponds to the highest relative trend (0.48%/yr). Weather-driven trends are statistically significant over most of the domain (18.9% and 46.9% of land areas have respectively highly and moderately significant trends), with non-significant areas (p-value$\geq$0.1) limited to the United Kingdom, Ireland, large parts of France, and parts of Germany, Italy, Portugal, and Spain. Significant trends are predominantly positive and particularly pronounced in the eastern half of the domain, exceeding 0.005 μg/m^3/yr in regions with high biogenic emissions. Since SOA is mainly present during summer (with aged primary organic aerosol considered as PAA), regression analyses between summertime SOA concentrations and summertime temperatures reveal significant correlations across the EUR domain (average R^2=0.46), highlighting the strong influence of summer temperature on SOA variability.

Temperature and LAI, both key factors affecting biogenic emissions, were identified as the primary drivers of annual SOA concentrations. While increasing temperatures can enhance biogenic emissions, they may also negatively affect the gas–particle partitioning of SVOCs. According to the multilinear model, SOA concentrations generally increase with annual temperature, with a modest population-weight rise across EUR of 0.032 μg/m^3/°C. Locally, very small negative trends with temperature are observed (5th percentile: -0.002 μg/m^3/°C), suggesting that in some areas higher temperatures may inhibit SOA formation. Temperature dominates the variability over most of the domain, whereas LAI is the primary driver across much of Scandinavia and Eastern Europe. In addition, solar radiation emerges as the dominant driver in certain regions of Eastern Europe.

It should be noted that although the model aims to represent SOA formation as accurately as possible, the results strongly depend on the estimation of biogenic emissions and the representation of SOA formation mechanisms, both of which remain uncertain. Missing or poorly characterized pathways (e.g. cloud chemistry) could lead to different weather-driven trends.

3.2.7 Primary natural Aerosol

Trends in sea salt concentrations over EUR are generally not statistically significant across most of the domain, with p-values exceeding 0.1. In a few areas, trends are marginally significant (p-values between 0.05 and 0.1), showing a slight negative change of approximately -0.005 μg/m^3/yr along the western coast of England and the southeastern coast of Italy. Statistically significant trends (p-value$<$0.05) are observed only in Turkey, with a positive trend exceeding 0.01 μg/m^3/yr around Istanbul. Similarly, trends in dust concentrations are largely nonsignificant across most of the domain but boundary conditions were held constant for this study.

Due to the lack of significant trends in dust and sea salt, weather-driven trends in fungal spore particles (illustrated in Fig. 15) largely drive the trends in natural primary particles. Fungal spore trends are of the same order of magnitude as SOA,

https://doi.org/10.5194/egusphere-2026-4644
Preprint. Discussion started: 9 September 2026

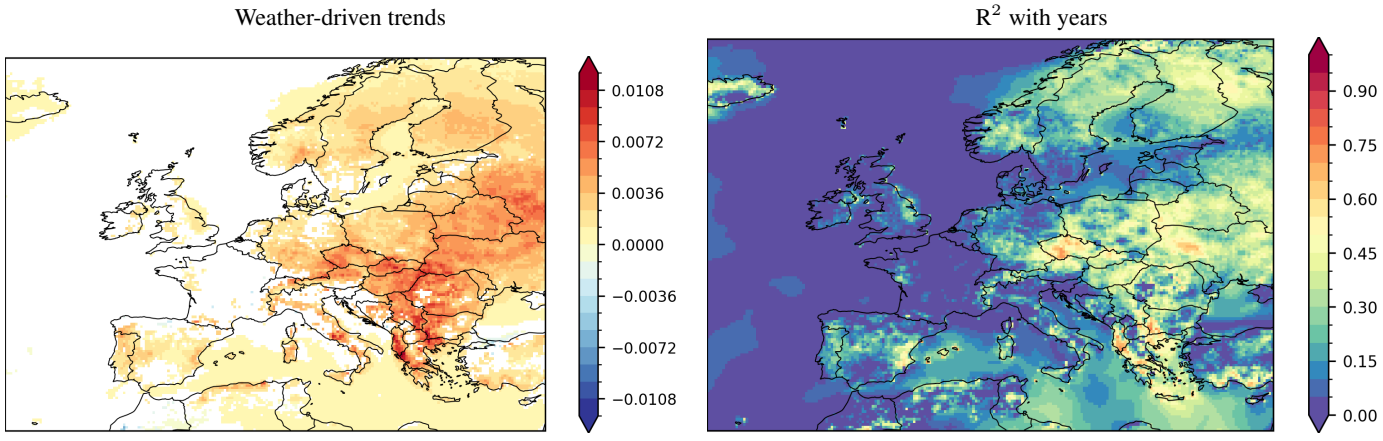

Figure 15. Maps of weather-driven trends and the corresponding R^2 over Europe for annual fungal spore concentrations.

with a positive population-weighted trend of 0.0019 μg/m^3/yr, corresponding to a relative increase of 0.4%/yr. The trends are consistent with the weather-driven trends of fungal spore emissions (illustrated by Fig. S15) and of LAI (illustrated by Fig. 1b), showing relatively high increases over Eastern Europe. Trends of concentrations around regions where fungal spore emission trends are negative due to a decrease in LAI (like in part of France, Northern Spain and Croatia) are generally nonsignificant, except very locally.

Fungal spores emissions are driven by the evolution of LAI and specific humidity. However, as relative humidity was used instead of specific humidity to avoid correlation between annual specific humidity and annual temperature, the multilinear model indicates that the trends of fungal spores are dominated by the trends of 2 factors: LAI and temperature, with LAI being the dominant factor at the scale of Europe. LAI is also the main driver of the variability of concentrations.

3.3 Weather-driven evolution of atmospheric deposition

A positive trend (cumulated over EUR) of 3.45 kT/yr (around 0.15%/yr, p-value$<$0.001, representing an increase of +4.8% over the period) is obtained for total (dry+wet) deposition of reduced nitrogen ($N_{reduced}$) mainly due to an increase in dry deposition (2.51 kT/yr, p-value$<$0.001), while the cumulative trend in wet deposition was found to be nonsignificant. The dry and wet cumulated trends over EUR of $N_{oxidized}$ and $S_{oxidized}$ are all statistically nonsignificant. Fig. 16 shows the spatial distribution of trends for wet and dry deposition. The spatial deposition of total (wet+dry) deposition and the maps of dominant drivers are also shown in supplementary materials (Figures S32 to S35).

Significant $N_{reduced}$ dry deposition positive weather-driven trends are simulated across a large part of the domain (around 60%), with the exception of Turkey where negative significant trends are simulated (a significant increase in the PBL is simulated over this region, leading to more vertical mixing and less dry deposition). The increase in $N_{reduced}$ dry deposition is primarily driven by rising temperatures, consistent with the temperature-induced increase in NH_3 emissions and changes in ammonia gas–particle partitioning. Higher temperatures and lower relative humidity both inhibit ammonium formation, result-

https://doi.org/10.5194/egusphere-2026-4644
Preprint. Discussion started: 9 September 2026

ing in more NH_3 remaining in the gas phase. Since gases generally deposit faster than submicron particles, these conditions tend to reduce the dry deposition rate of $N_{reduced}$. At the EUR scale, sensitivity simulations comparing selected cold and hot years indicate that the temperature effect on emissions likely accounts for most of the weather-driven trend, explaining approximately 70% of the differences between hot and cold years (average increase over EUR of 21.1 mg-N/m^2 with dynamic emissions against 6.3 mg-N/m^2 without).

The trends of $N_{reduced}$ wet deposition have a complex spatial pattern. Trends were found to increase in areas close to emission hotspots (especially in Northern Italy, Northeastern Spain, Western France, Austria and Southeastern Europe) but decrease in others (especially in Northeastern France, Southern Germany, Romania, Belarus, Ukraine and Lithuania). Although the multilinear model indicates that multiple drivers contribute to the trends of $N_{reduced}$ wet deposition (changes in temperature, wind direction, and relative humidity) over these regions, the multilinear model rarely indicates that precipitation is the main driver due to the lack of significant interannual trend for precipitations. Temperature is always the dominant factor and is mainly associated with an increase in wet deposition, consistently with the increase in ammonia emissions.

However, wet deposition of $N_{reduced}$ generally increases between the selected cold and hot years when emissions are assumed to be meteorology-dependent (+11.4 mg-N/m^2, increasing annual ammonia emissions), but predominantly decreases when emissions are meteorology-independent (-10.9 mg-N/m^2, constant annual ammonia emissions). This contrast indicates that although rising temperatures enhance ammonia emissions, the efficiency of wet deposition simultaneously decreases. This behavior may result partly from the competition between dry and wet deposition processes, as enhanced dry deposition (which increases by 6.3 mg-N/m^2 with constant annual ammonia emissions) reduces the amount of $N_{reduced}$ available in the atmosphere for wet removal. In addition, in-cloud scavenging of ammonia can become less efficient at higher temperatures, since in CHIMERE it is parameterized through ammonia absorption by cloud water using Henry's law, with solubility decreasing as temperature increases.

The worsening of $N_{reduced}$ deposition is consistent with the findings of Simpson et al. (2014), who reported that climate-induced increases in NH_3 emissions could exacerbate exceedances of critical loads. In particular, they showed that a 30% increase in NH_3 emissions may lead to a 57% increase in areas exceeding critical loads for $N_{reduced}$.

Spatial patterns of dry deposition for $N_{oxidized}$ are similar to those of $N_{reduced}$, although the associated trends are less pronounced. Increases in $N_{oxidized}$ deposition are mainly observed over central Europe, with the largest increases (around 1 mg-N/m^2) occurring in the Netherlands and eastern Germany. In contrast, some localized statistically significant decreases are simulated in the Po Valley. Temperature emerges as the dominant driver of these trends. However, its influence is twofold. While rising temperatures increase $N_{oxidized}$ dry deposition velocities by limiting nitrate formation, in a manner analogous to $N_{reduced}$, they simultaneously lead to reductions in NOx emissions. Sensitivity simulations reveal a substantially larger increase in $N_{oxidized}$ dry deposition between cold and hot years when emissions are assumed to be meteorology-independent (mean increase over EUR of 17.2 mg-N/m^2) compared with simulations using meteorology-dependent emissions (9.6 mg-N/m^2). For $N_{oxidized}$ wet deposition, the model simulates strong increases over Denmark ($>$ 1 mg-N/m^2/yr), more moderate localized increases over Italy and Greece, and decreases across the eastern part of the domain.

https://doi.org/10.5194/egusphere-2026-4644
Preprint. Discussion started: 9 September 2026

For $S_{oxidized}$, deposition trends are generally nonsignificant, except locally around some SO_2 hotspots. Around these hotspots, trends of dry deposition are generally slightly positive (likely related to an increase in the oxidation rate of SO_2 into sulfate particles) while trends for wet deposition are generally negative (likely due to a less efficient wet deposition), leading to trends of total deposition that are generally negative.

4 Conclusions

An improved version of CHIMERE v2020r1 was developed in order to better represent the dependence of atmospheric emissions, concentrations and deposition to meteorological drivers. This version especially includes meteorology-dependent anthropogenic emissions, varying 8-day leaf area index from satellite data over the whole period, and updated parameterizations for deposition as well as soil and biogenic emissions.

Simulations were performed in order to isolate the influence of meteorology on emissions (both natural and anthropogenic), atmospheric concentrations of main pollutants (O_3, SOMO35, NO_2, PM), and on the deposition of acidifying and eutrophizing compounds during the 1990-2022 period in Europe.

The results show a strong effect of annual temperature on emissions. An increase in temperature was found to lead to an increase in biogenic VOC, fungal spores, NH_3 and soil NO_x emissions and to a decrease in anthropogenic NO_x and PM emissions.

These effects on emissions combined with the effect of meteorology led to a complex impact on atmospheric concentrations and deposition. The weather-driven trends of atmospheric concentrations and deposition were therefore analyzed with a multilinear regression approach (including different meteorological variables, the LAI vegetation index and the deposition velocity) to determine the main drivers. For annual O_3 concentrations, annual temperatures, LAI and deposition velocities are significant drivers. Although annual O_3 concentrations increase over a large part of Europe as a result of rising temperatures during the simulation period, negative trends are simulated in regions where deposition velocities increase. Significant increases, driven mainly by rising temperatures and solar radiation, are simulated for SOMO35 and AOT40c, with population-weighted trends of 0.5%/yr and 0.69%/yr, corresponding to overall increases by 18% and 22% over the 1990–2022 period, respectively. For NO_2 concentrations, a negative trend was simulated over part of southern Europe due to the accounted effect of temperature on emissions.

For particles, a negative trend, dominated by the decrease in PAA and SIA concentrations, over most of Europe largely due to rising temperatures reducing NO_x and primary PM emissions but also limiting the formation of ammonium nitrate. However, other drivers (like relative humidity and wind direction) also influence primary PM and SIA weather-driven trends. Positive trends are simulated in Northern and Eastern Europe due to an increase in SOA and spore concentrations due to an increase in biogenic emissions (linked to increases in LAI and temperature). A strong increase in $N_{reduced}$ deposition was also simulated in almost all Europe, mainly due to the increase in ammonia emissions.

Accurately accounting for the effect of meteorological parameters on emissions was proved to be critical in determining trends. A key methodological outcome of this study is that accurately accounting for the meteorological dependence of emis-

https://doi.org/10.5194/egusphere-2026-4644
Preprint. Discussion started: 9 September 2026

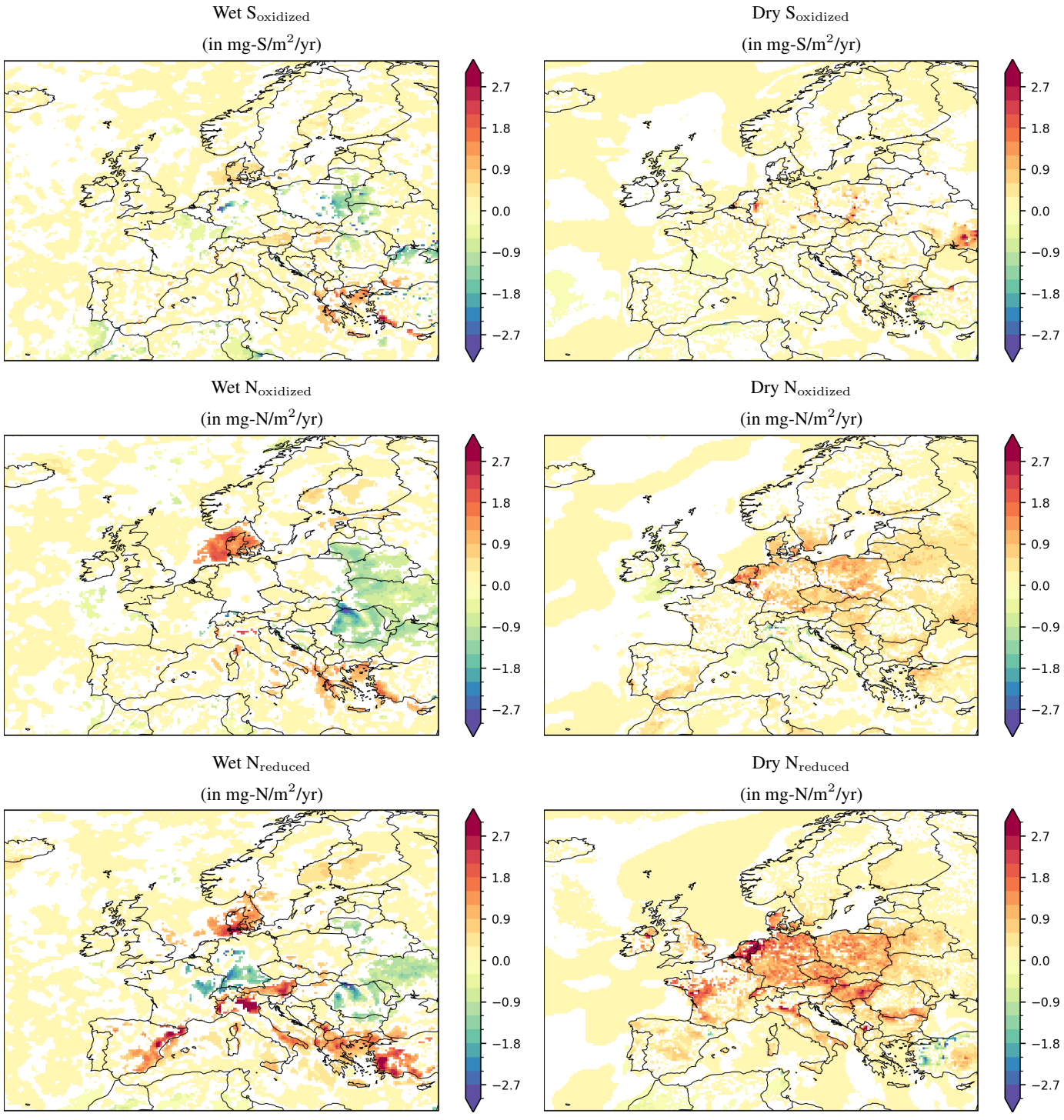

Figure 16. Maps of weather-driven trends for dry and wet deposition of SOx, NOx and NHx.

https://doi.org/10.5194/egusphere-2026-4644
Preprint. Discussion started: 9 September 2026

sions is essential to correctly assess weather-driven trends. The results demonstrate that temperature-induced changes in both anthropogenic and natural emissions (including NO_x, NH_3, primary PM, and biogenic VOCs) strongly control the magnitude and even the sign of simulated trends in atmospheric concentrations and deposition. In particular, the negative weather-driven trends in primary particles and secondary inorganic aerosols, as well as the positive trends in reduced nitrogen deposition, would be miscalculated if emissions were assumed to be independent of meteorological conditions. Consequently, studies focusing on the impact of climate change on air quality should therefore incorporate dynamic emissions accounting for the effect of all meteorological parameters.

Code availability. The version of the CHIMERE model developed in this study is available upon request.

Data availability. Simulation results for annual emissions, concentrations, and deposition are available at https://zenodo.org/records/21718960.

Author contributions. FC, AG, AC and RM conceptualized the work. FC developed the new CHIMERE version. FC, AG, PM, ER and GD performed the simulations. FC did the analysis, and wrote the manuscript. All authors reviewed the manuscript before submission.

Competing interests. The contact author has declared that none of the authors has any competing interests.

Acknowledgements. This work has been carried out thanks to the support of the projects (RECAPS/Primequal and ECLAT/AQACIA projects) funded by ADEME and Support from French Ministry in charge of ecology.

https://doi.org/10.5194/egusphere-2026-4644
Preprint. Discussion started: 9 September 2026

References

Bauwens, M., Stavrakou, T., Müller, J.-F., Van Schaeybroeck, B., De Cruz, L., De Troch, R., Giot, O., Hamdi, R., Termonia, P., Laffineur, Q., Amelynck, C., Schoon, N., Heinesch, B., Holst, T., Arneth, A., Ceulemans, R., Sanchez-Lorenzo, A., and Guenther, A.: Recent past (1979–2014) and future (2070–2099) isoprene fluxes over Europe simulated with the MEGAN–MOHYCAN model, Biogeosciences, 15, 3673–3690, https://doi.org/10.5194/bg-15-3673-2018, 2018.

Bonan, G. B., Patton, E. G., Harman, I. N., Oleson, K. W., Finnigan, J. J., Lu, Y., and Burakowski, E. A.: Modeling canopy-induced turbulence in the Earth system: a unified parameterization of turbulent exchange within plant canopies and the roughness sublayer (CLM-ml v0), Geosci. Model Dev., 11, 1467–1496, https://doi.org/10.5194/gmd-11-1467-2018, 2018.

Carnicer, J., Alegria, A., Giannakopoulos, C., Di Giuseppe, F., Karali, A., Koutsias, N., Lionello, P., Parrington, M., and Vitolo, C.: Global warming is shifting the relationships between fire weather and realized fire-induced CO2 emissions in Europe, Sci. Rep., 12, 10 365, https://doi.org/0.1038/s41598-022-14480-8, 2022.

Cholakian, A., Colette, A., Coll, I., Ciarelli, G., and Beekmann, M.: Future climatic drivers and their effect on PM_{10} components in Europe and the Mediterranean Sea, Atmos. Chem. Phys., 19, 4459–4484, https://doi.org/10.5194/acp-19-4459-2019, 2019.

Chrit, M., Sartelet, K., Sciare, J., Pey, J., Marchand, N., Couvidat, F., Sellegri, K., and Beekmann, M.: Modelling organic aerosol concentrations and properties during ChArMEx summer campaigns of 2012 and 2013 in the western Mediterranean region, Atmos. Chem. Phys., 17, 12 509–12 531, https://doi.org/10.5194/acp-17-12509-2017, 2017.

Ciccioli, P., Silibello, C., Finardi, S., Pepe, N., Ciccioli, P., Rapparini, F., Neri, L., Fares, S., Brilli, F., Mircea, M., Magliulo, E., and Baraldi, R.: The potential impact of biogenic volatile organic compounds (BVOCs) from terrestrial vegetation on a Mediterranean area using two different emission models, Agric. For. Meteor., 328, 109 255, https://doi.org/10.1016/j.agrformet.2022.109255, 2023.

Clifton, O. E., Paulot, F., Fiore, A. M., Horowitz, L. W., Correa, G., Baublitz, C. B., Fares, S., Goded, I., Goldstein, A. H., Gruening, C., Hogg, A. J., Loubet, B., Mammarella, I., Munger, J. W., Neil, L., Stella, P., Uddling, J., Vesala, T., and Weng, E.: Influence of Dynamic Ozone Dry Deposition on Ozone Pollution, J. Geophys. Res. Atmos., 125, e2020JD032 398, https://doi.org/10.1029/2020JD032398, 2020.

CLMS: European Union's Copernicus Land Monitoring Service information, CORINE Land Cover 2018 (raster 100 m), Europe, 6-yearly - version 2020_20u1, May 2020, https://doi.org/10.2909/960998c1-1870-4e82-8051-6485205ebbac, 2020.

Coelho, S., Rafael, S., Lopes, D., Miranda, A., and Ferreira, J.: How changing climate may influence air pollution control strategies for 2030?, Sci. Total Environ., 758, 143 911, https://doi.org/https://doi.org/10.1016/j.scitotenv.2020.143911, 2021.

Colette, A., Bessagnet, B., Vautard, R., Szopa, S., Rao, S., Schucht, S., Klimont, Z., Menut, L., Clain, G., Meleux, F., Curci, G., and Rouïl, L.: European atmosphere in 2050, a regional air quality and climate perspective under CMIP5 scenarios, Atmos. Chem. Phys., 13, 7451–7471, https://doi.org/10.5194/acp-13-7451-2013, 2013.

Couvidat, F., Bessagnet, B., Garcia-Vivanco, M., Real, E., Menut, L., and Colette, A.: Development of an inorganic and organic aerosol model (CHIMERE 2017β v1.0): seasonal and spatial evaluation over Europe, Geosci. Model Dev., 11, 165–194, https://doi.org/10.5194/gmd-11-165-2018, 2018.

Cuevas-Agulló, E., Barriopedro, D., García, R. D., Alonso-Pérez, S., González-Alemán, J. J., Werner, E., Suárez, D., Bustos, J. J., García-Castrillo, G., García, O., Barreto, A., and Basart, S.: Sharp increase in Saharan dust intrusions over the western Euro-Mediterranean in February–March 2020–2022 and associated atmospheric circulation, Atmos. Chem. Phys., 24, 4083–4104, https://doi.org/10.5194/acp-24-4083-2024, 2024.

https://doi.org/10.5194/egusphere-2026-4644
Preprint. Discussion started: 9 September 2026

ECMWF: IFS documentation – Cy43r1. Operational implementation 22 Nov 2016. Part IV. Physical Processes., Tech. rep., European Centre for Medium-Range Weather Forecasts, 2016.

EEA: The European air quality observation network AQ e-Reporting, https://www.eea.europa.eu/en/datahub/datahubitem-view/3b390c9c-f321-490a-b25a-ae93b2ed80c1, 2023.

Emberson, L. D., Simpson, D., Tuovinen, J. P., Ashmore, M. R., and Cambridge, H. M.: Towards a model of ozone deposition and stomatal uptake over Europe, Tech. rep., EMEP/MSC-W, 2000.

Eyring, V., Arblaster, J. M., Cionni, I., Sedláček, J., Perlwitz, J., Young, P. J., Bekki, S., Bergmann, D., Cameron-Smith, P., Collins, W. J., Faluvegi, G., Gottschaldt, K.-D., Horowitz, L. W., Kinnison, D. E., Lamarque, J.-F., Marsh, D. R., Saint-Martin, D., Shindell, D. T., Sudo, K., Szopa, S., and Watanabe, S.: Long-term ozone changes and associated climate impacts in CMIP5 simulations, Journal of Geophysical Research: Atmospheres, 118, 5029–5060, https://doi.org/10.1002/jgrd.50316, 2013.

Fiore, A. M., Naik, V., Spracklen, D. V., Steiner, A., Unger, N., Prather, M., Bergmann, D., Cameron-Smith, P. J., Cionni, I., Collins, W. J., Dalsøren, S., Eyring, V., Folberth, G. A., Ginoux, P., Horowitz, L. W., Josse, B., Lamarque, J.-F., MacKenzie, I. A., Nagashima, T., O'Connor, F. M., Righi, M., Rumbold, S. T., Shindell, D. T., Skeie, R. B., Sudo, K., Szopa, S., Takemura, T., and Zeng, G.: Global air quality and climate, Chem. Soc. Rev., 41, 6663–6683, https://doi.org/10.1039/C2CS35095E, 2012.

Gao, Y., Fu, J. S., Drake, J. B., Lamarque, J.-F., and Liu, Y.: The impact of emission and climate change on ozone in the United States under representative concentration pathways (RCPs), Atmos. Chem. Phys., 13, 9607–9621, https://doi.org/10.5194/acp-13-9607-2013, 2013.

Gelaro, R., McCarty, W., Suárez, M. J., Todling, R., Molod, A., Takacs, L., Randles, C. A., Darmenov, A., Bosilovich, M. G., Reichle, R., Wargan, K., Coy, L., Cullather, R., Draper, C., Akella, S., Buchard, V., Conaty, A., da Silva, A. M., Gu, W., Kim, G.-K., Koster, R., Lucchesi, R., Merkova, D., Nielsen, J. E., Partyka, G., Pawson, S., Putman, W., Rienecker, M., Schubert, S. D., Sienkiewicz, M., and Zhao, B.: The Modern-Era Retrospective Analysis for Research and Applications, Version 2 (MERRA-2), J. Clim., 30, 5419 – 5454, https://doi.org/10.1175/JCLI-D-16-0758.1, 2017.

Global Soil Data Task: Global Soil Data Products CD-ROM Contents (IGBP-DIS), https://doi.org/10.3334/ORNLDAAC/565, 2000.

Grange, S. K., Farren, N. J., Vaughan, A. R., Rose, R. A., and Carslaw, D. C.: Strong Temperature Dependence for Light-Duty Diesel Vehicle NOx Emissions, Environ. Sci. Technol., 53, 6587–6596, https://doi.org/10.1021/acs.est.9b01024, 2019.

Guenther, A.: MEGAN 3.2 input files [Data set], https://doi.org/10.5281/zenodo.10939297, 2024.

Guenther, A. B., Jiang, X., Heald, C. L., Sakulyanontvittaya, T., Duhl, T., Emmons, L. K., and Wang, X.: The Model of Emissions of Gases and Aerosols from Nature version 2.1 (MEGAN2.1): an extended and updated framework for modeling biogenic emissions, Geosci. Model Dev., 5, 1471–1492, https://doi.org/10.5194/gmd-5-1471-2012, 2012.

Guevara, M., Jorba, O., Tena, C., Denier van der Gon, H., Kuenen, J., Elguindi, N., Darras, S., Granier, C., and Pérez García-Pando, C.: Copernicus Atmosphere Monitoring Service TEMPOral profiles (CAMS-TEMPO): global and European emission temporal profile maps for atmospheric chemistry modelling, Earth Syst. Sci. Data, 13, 367–404, https://doi.org/10.5194/essd-13-367-2021, 2021.

Guion, A., Turquety, S., Polcher, J., Pennel, R., Bastin, S., and Arsouze, T.: Droughts and heatwaves in the Western Mediterranean: impact on vegetation and wildfires using the coupled WRF-ORCHIDEE regional model (RegIPSL)., Clim. Dyn., 58, https://doi.org/10.1007/s00382-021-05938-y, 2022.

Guion, A., Turquety, S., Cholakian, A., Polcher, J., Ehret, A., and Lathière, J.: Biogenic isoprene emissions, dry deposition velocity, and surface ozone concentration during summer droughts, heatwaves, and normal conditions in southwestern Europe, Atmos. Chem. Phys., 23, 1043–1071, https://doi.org/10.5194/acp-23-1043-2023, 2023.

https://doi.org/10.5194/egusphere-2026-4644
Preprint. Discussion started: 9 September 2026

Guion, A., Couvidat, F., Guevara, M., and Colette, A.: Country- and species-dependent parameters for the heating degree day method to distribute NOx and PM emissions from residential heating in the EU 27: application to air quality modelling and multi-year emission projections, Atmos. Chem. Phys., 25, 2807–2827, https://doi.org/10.5194/acp-25-2807-2025, 2025.

He, C., Kumar, R., Tang, W., Pfister, G., Xu, Y., Qian, Y., and Brasseur, G.: Air Pollution Interactions with Weather and Climate Extremes: Current Knowledge, Gaps, and Future Directions, Curr. Pollut. Rep., 10, 430–442, https://doi.org/10.1007/s40726-024-00296-9, 2024.

Heald, C. and Spracklen, D.: Atmospheric budget of primary biological aerosol particles from fungal spores. Geophys Res Lett 36: L09806, Geophys. Res. Lett., 36, L09 806, https://doi.org/10.1029/2009GL037493, 2009.

Heald, C. L., Henze, D. K., Horowitz, L. W., Feddema, J., Lamarque, J.-F., Guenther, A., Hess, P. G., Vitt, F., Seinfeld, J. H., Goldstein, A. H., and Fung, I.: Predicted change in global secondary organic aerosol concentrations in response to future climate, emissions, and land use change, J. Geophys. Res. Atmos., 113, https://doi.org/10.1029/2007JD009092, 2008.

Henrot, A.-J., Stanelle, T., Schröder, S., Siegenthaler, C., Taraborrelli, D., and Schultz, M. G.: Implementation of the MEGAN (v2.1) biogenic emission model in the ECHAM6-HAMMOZ chemistry climate model, Geosci. Model Dev., 10, 903–926, https://doi.org/10.5194/gmd-10-903-2017, 2017.

Hersbach, H., Bell, B., Berrisford, P., Hirahara, S., Horányi, A., Muñoz-Sabater, J., Nicolas, J., Peubey, C., Radu, R., Schepers, D., Simmons, A., Soci, C., Abdalla, S., Abellan, X., Balsamo, G., Bechtold, P., Biavati, G., Bidlot, J., Bonavita, M., De Chiara, G., Dahlgren, P., Dee, D., Diamantakis, M., Dragani, R., Flemming, J., Forbes, R., Fuentes, M., Geer, A., Haimberger, L., Healy, S., Hogan, R. J., Hólm, E., Janisková, M., Keeley, S., Laloyaux, P., Lopez, P., Lupu, C., Radnoti, G., de Rosnay, P., Rozum, I., Vamborg, F., Villaume, S., and Thépaut, J.-N.: The ERA5 global reanalysis, Q. J. R. Meteorol. Soc., 146, 1999–2049, https://doi.org/10.1002/qj.3803, 2020.

Houssami, N., Macaskill, P., Marinovich, M. L., Dixon, J. M., Irwig, L., Brennan, M. E., and Solin, L. J.: Meta-analysis of the impact of surgical margins on local recurrence in women with early-stage invasive breast cancer treated with breast-conserving therapy, Eur. J. Cancer, 46, 3219–3232, https://doi.org/https://doi.org/10.1016/j.ejca.2010.07.043, 2010.

Hussain, M. and Mahmud, I.: pyMannKendall: a python package for non parametric Mann Kendall family of trend tests., J. Open Source Softw., 4, 1556, https://doi.org/10.21105/joss.01556, 2019.

Jacob, D. J. and Winner, D. A.: Effect of climate change on air quality, Atmospheric Environment, 43, 51–63, https://doi.org/10.1016/j.atmosenv.2008.09.051, 2009.

Jiang, J., Aksoyoglu, S., Ciarelli, G., Oikonomakis, E., El-Haddad, I., Canonaco, F., O'Dowd, C., Ovadnevaite, J., Minguillón, M. C., Baltensperger, U., and Prévôt, A. S. H.: Effects of two different biogenic emission models on modelled ozone and aerosol concentrations in Europe, Atmos. Chem. Phys., 19, 3747–3768, https://doi.org/10.5194/acp-19-3747-2019, 2019.

Jiang, J., Stevenson, D., Uwizeye, A., Casu, F. A. M., Tempio, G., Falcucci, A., and Sutton, M. A.: Global warming increases ammonia emissions and reduces the efficacy of mitigation actions, Commun. Earth. Environ., 7, 398, https://doi.org/0.1038/s43247-026-03404-3, 2026.

Jones, M. W., Abatzoglou, J. T., Veraverbeke, S., Andela, N., Lasslop, G., Forkel, M., Smith, A. J. P., Burton, C., Betts, R. A., van der Werf, G. R., Sitch, S., Canadell, J. G., Santín, C., Kolden, C., Doerr, S. H., and Le Quéré, C.: Global and Regional Trends and Drivers of Fire Under Climate Change, Rev. Geophys., 60, e2020RG000 726, https://doi.org/10.1029/2020RG000726, 2022.

Jones, M. W., Veraverbeke, S., Andela, N., Doerr, S. H., Kolden, C., Mataveli, G., Pettinari, M. L., Quéré, C. L., Rosan, T. M., van der Werf, G. R., van Wees, D., and Abatzoglou, J. T.: Global rise in forest fire emissions linked to climate change in the extratropics, Science, 386, eadl5889, https://doi.org/10.1126/science.adl5889, 2024.

https://doi.org/10.5194/egusphere-2026-4644
Preprint. Discussion started: 9 September 2026

Jongh, P. D., Jongh, E. D., and Santana, L.: The impact of pre-selected variance inflation factor thresholds on the stability and predictive power of logistic regression models in credit scoring, ORiON, 31, 17–37, https://doi.org/10.5784/31-1-162, 2015.

Katragkou, E., Zanis, P., Kioutsioukis, I., Tegoulias, I., Melas, D., Krüger, B. C., and Coppola, E.: Future climate change impacts on summer surface ozone from regional climate-air quality simulations over Europe, J. Geophys. Res. Atmos., 116, D22 307, https://doi.org/10.1029/2011JD015899, 2011.

Kuenen, J., Dellaert, S., Visschedijk, A., Jalkanen, J.-P., Super, I., and Denier van der Gon, H.: CAMS-REG-v4: a state-of-the-art high-resolution European emission inventory for air quality modelling, Earth Syst. Sci. Data, 14, 491–515, https://doi.org/10.5194/essd-14-491-2022, 2022.

Laanaia, N., Carrer, D., Calvet, J.-C., and Pagé, C.: How will climate change affect the vegetation cycle over France? A generic modeling approach, Clim. Risk Manag., 13, 31–42, https://doi.org/10.1016/j.crm.2016.06.001, 2016.

Lan, X. and Keeling, R.: Data downloaded on https://gml.noaa.gov/ccgg/trends/ and produced by NOAA/GML and the Scripps Institution of Oceanography. Last access: September 16^{th} 2024, 2024.

Lin, G., Penner, J. E., and Zhou, C.: How will SOA change in the future?, Geophys. Res. Lett., 43, 1718–1726, https://doi.org/10.1002/2015GL067137, 2016.

Lin, Y., Zhang, L., Fan, Q., Meng, H., Gao, Y., Gao, H., and Yao, X.: Decoupling impacts of weather conditions on interannual variations in concentrations of criteria air pollutants in South China – constraining analysis uncertainties by using multiple analysis tools, Atmos. Chem. Phys., 22, 16 073–16 090, https://doi.org/10.5194/acp-22-16073-2022, 2022.

Liu, Y., Liu, R., and Chen, J. M.: Retrospective retrieval of long-term consistent global leaf area index (1981–2011) from combined AVHRR and MODIS data, J. Geophys. Res. Biogeo., 117, G04 003, https://doi.org/10.1029/2012JG002084, 2012.

Mailler, S., Menut, L., Khvorostyanov, D., Valari, M., Couvidat, F., Siour, G., Turquety, S., Briant, R., Tuccella, P., Bessagnet, B., Colette, A., Létinois, L., Markakis, K., and Meleux, F.: CHIMERE-2017: from urban to hemispheric chemistry-transport modeling, Geosci. Model Dev., 10, 2397–2423, https://doi.org/10.5194/gmd-10-2397-2017, 2017.

Massad, R.-S., Nemitz, E., and Sutton, M. A.: Review and parameterisation of bi-directional ammonia exchange between vegetation and the atmosphere, Atmos. Chem. Phys., 10, 10 359–10 386, https://doi.org/10.5194/acp-10-10359-2010, 2010.

Megaritis, A. G., Fountoukis, C., Charalampidis, P. E., Denier van der Gon, H. A. C., Pilinis, C., and Pandis, S. N.: Linking climate and air quality over Europe: effects of meteorology on $PM_{2.5}$ concentrations, Atmos. Chem. Phys., 14, 10 283–10 298, https://doi.org/10.5194/acp-14-10283-2014, 2014.

Meleux, F., Solmon, F., and Giorgi, F.: Increase in summer European ozone amounts due to climate change, Atmos. Environ., 41, 7577–7587, https://doi.org/10.1016/j.atmosenv.2007.05.048, 2007.

Menut, L., Bessagnet, B., Briant, R., Cholakian, A., Couvidat, F., Mailler, S., Pennel, R., Siour, G., Tuccella, P., Turquety, S., and Valari, M.: The CHIMERE v2020r1 online chemistry-transport model, Geosci. Model Dev., 14, 6781–6811, https://doi.org/10.5194/gmd-14-6781-2021, 2021.

Messina, P., Lathière, J., Sindelarova, K., Vuichard, N., Granier, C., Ghattas, J., Cozic, A., and Hauglustaine, D. A.: Global biogenic volatile organic compound emissions in the ORCHIDEE and MEGAN models and sensitivity to key parameters, Atmos. Chem. Phys., 16, 14 169–14 202, https://doi.org/10.5194/acp-16-14169-2016, 2016.

Mu, Q., Denby, B. R., Wærsted, E. G., and Fagerli, H.: Downscaling of air pollutants in Europe using uEMEP_v6, Geosci. Model Dev., 15, 449–465, https://doi.org/10.5194/gmd-15-449-2022, 2022.

https://doi.org/10.5194/egusphere-2026-4644
Preprint. Discussion started: 9 September 2026

Müller, J.-F., Stavrakou, T., Wallens, S., De Smedt, I., Van Roozendael, M., Potosnak, M. J., Rinne, J., Munger, B., Goldstein, A., and Guenther, A. B.: Global isoprene emissions estimated using MEGAN, ECMWF analyses and a detailed canopy environment model, Atmos. Chem. Phys., 8, 1329–1341, https://doi.org/10.5194/acp-8-1329-2008, 2008.

Otero, N., Sillmann, J., Mar, K. A., Rust, H. W., Solberg, S., Andersson, C., Engardt, M., Bergström, R., Bessagnet, B., Colette, A., Couvidat, F., Cuvelier, C., Tsyro, S., Fagerli, H., Schaap, M., Manders, A., Mircea, M., Briganti, G., Cappelletti, A., Adani, M., D'Isidoro, M., Pay, M.-T., Theobald, M., Vivanco, M. G., Wind, P., Ojha, N., Raffort, V., and Butler, T.: A multi-model comparison of meteorological drivers of surface ozone over Europe, Atmos. Chem. Phys., 18, 12 269–12 288, https://doi.org/10.5194/acp-18-12269-2018, 2018.

Rasmussen, D. J., Hu, J., Mahmud, A., and Kleeman, M. J.: The Ozone–Climate Penalty: Past, Present, and Future, Environ. Sci. Technol., 47, 14 258–14 266, https://doi.org/10.1021/es403446m, 2013.

Sartelet, K., Couvidat, F., Wang, Z., Flageul, C., and Kim, Y.: SSH-Aerosol v1. 1: A Modular Box Model to Simulate the Evolution of Primary and Secondary Aerosols, Atmosphere, 11, 525, https://doi.org/10.3390/atmos11050525, 2020.

Sillanpää, S., Fung, P., Niemi, J., Kousa, A., Kangas, L., Zaidan, M., Timonen, H., Kulmala, M., and Petäjä, T.: Long-term air quality trends of regulated pollutants in the Helsinki metropolitan area from 1994–2019 and its implications to the Air Quality Index., Boreal Environ. Res., 27, 61–79, 2022.

Simpson, D., Benedictow, A., Berge, H., Bergström, R., Emberson, L. D., Fagerli, H., Flechard, C. R., Hayman, G. D., Gauss, M., Jonson, J. E., Jenkin, M. E., Nyíri, A., Richter, C., Semeena, V. S., Tsyro, S., Tuovinen, J.-P., Valdebenito, A., and Wind, P.: The EMEP MSC-W chemical transport model; technical description, Atmos. Chem. Phys., 12, 7825–7865, https://doi.org/10.5194/acp-12-7825-2012, 2012.

Simpson, D., Andersson, C., Christensen, J. H., Engardt, M., Geels, C., Nyiri, A., Posch, M., Soares, J., Sofiev, M., Wind, P., and Langner, J.: Impacts of climate and emission changes on nitrogen deposition in Europe: a multi-model study, Atmos. Chem. Phys., 14, 6995–7017, https://doi.org/10.5194/acp-14-6995-2014, 2014.

Skjøth, C. A., Geels, C., Berge, H., Gyldenkærne, S., Fagerli, H., Ellermann, T., Frohn, L. M., Christensen, J., Hansen, K. M., Hansen, K., and Hertel, O.: Spatial and temporal variations in ammonia emissions – a freely accessible model code for Europe, Atmos. Chem. Phys., 11, 5221–5236, https://doi.org/10.5194/acp-11-5221-2011, 2011.

Stowell, J. D., min Kim, Y., Gao, Y., Fu, J. S., Chang, H. H., and Liu, Y.: The impact of climate change and emissions control on future ozone levels: Implications for human health, Environment International, 108, 41–50, https://doi.org/10.1016/j.envint.2017.08.001, 2017.

Sutton, M. A., Reis, S., Riddick, S. N., Dragosits, U., Nemitz, E., Theobald, M. R., Tang, Y. S., Braban, C. F., Vieno, M., Dore, A. J., Mitchell, R. F., Wanless, S., Daunt, F., Fowler, D., Blackall, T. D., Milford, C., Flechard, C. R., Loubet, B., Massad, R., Cellier, P., Personne, E., Coheur, P. F., Clarisse, L., Van Damme, M., Ngadi, Y., Clerbaux, C., Skjøth, C. A., Geels, C., Hertel, O., Wichink Kruit, R. J., Pinder, R. W., Bash, J. O., Walker, J. T., Simpson, D., Horváth, L., Misselbrook, T. H., Bleeker, A., Dentener, F., and de Vries, W.: Towards a climate-dependent paradigm of ammonia emission and deposition, Philosophical Transactions of the Royal Society B: Biological Sciences, 368, 20130 166, https://doi.org/10.1098/rstb.2013.0166, 2013.

Tagaris, E., Manomaiphiboon, K., Liao, K.-J., Leung, L. R., Woo, J.-H., He, S., Amar, P., and Russell, A. G.: Impacts of global climate change and emissions on regional ozone and fine particulate matter concentrations over the United States, J. Geophys. Res. Atmos., 112, 14 312, https://doi.org/10.1029/2006JD008262, 2007.

Turco, M., Bedia, J., Di Liberto, F., Fiorucci, P., von Hardenberg, J., Koutsias, N., Llasat, M.-C., Xystrakis, F., and Provenzale, A.: Decreasing Fires in Mediterranean Europe, PLOS ONE, 11, 1–19, https://doi.org/10.1371/journal.pone.0150663, 2016.

https://doi.org/10.5194/egusphere-2026-4644
Preprint. Discussion started: 9 September 2026

van Caspel, W. E., Klimont, Z., Heyes, C., and Fagerli, H.: Impact of methane and other precursor emission reductions on surface ozone in Europe: scenario analysis using the European Monitoring and Evaluation Programme (EMEP) Meteorological Synthesizing Centre – West (MSC-W) model, Atmos. Chem. Phys., 24, 11 545–11 563, https://doi.org/10.5194/acp-24-11545-2024, 2024.

Venäläinen, A., Korhonen, N., Hyvärinen, O., Koutsias, N., Xystrakis, F., Urbieta, I. R., and Moreno, J. M.: Temporal variations and change in forest fire danger in Europe for 1960–2012, Nat. Hazards Earth Syst. sci., 14, 1477–1490, https://doi.org/10.5194/nhess-14-1477-2014, 2014a.

Venäläinen, A., Korhonen, N., Hyvärinen, O., Koutsias, N., Xystrakis, F., Urbieta, I. R., and Moreno, J. M.: Temporal variations and change in forest fire danger in Europe for 1960–2012, Nat. hazards earth syst. sci., 14, 1477–1490, https://doi.org/10.5194/nhess-14-1477-2014, 2014b.

Vida, M., Foret, G., Siour, G., Couvidat, F., Favez, O., Uzu, G., Cholakian, A., Conil, S., Beekmann, M., and Jaffrezo, J.-L.: Modelling of atmospheric concentrations of fungal spores: a 2-year simulation over France using CHIMERE, Atmos. Chem. Phys., 24, 10 601–10 615, https://doi.org/10.5194/acp-24-10601-2024, 2024.

Wang, H., Liu, X., Wu, C., and Lin, G.: Regional to global distributions, trends, and drivers of biogenic volatile organic compound emission from 2001 to 2020, Atmos. Chem. Phys., 24, 3309–3328, https://doi.org/10.5194/acp-24-3309-2024, 2024a.

Wang, Z., Couvidat, F., and Sartelet, K.: Response of biogenic secondary organic aerosol formation to anthropogenic NOx emission mitigation, Sci. Total Environ., p. 172142, https://doi.org/10.1016/j.scitotenv.2024.172142, 2024b.

Wesely, M.: Parameterization of surface resistances to gaseous dry deposition in regional-scale numerical models, Atmos. Environ., 23, 1293–1304, https://doi.org/10.1016/0004-6981(89)90153-4, 1989.

Wu, Q., Wang, X., Chen, S., Wang, L., and Jiang, J.: Land Surface Greening and CO2 Fertilization More than Offset the Gross Carbon Sequestration Decline Caused by Land Cover Change and the Enhanced Vapour Pressure Deficit in Europe, Remote Sensing, 15, 1372, https://doi.org/10.3390/rs15051372, 2023.

Wu, W., Fu, T.-M., Arnold, S. R., Spracklen, D. V., Zhang, A., Tao, W., Wang, X., Hou, Y., Mo, J., Chen, J., Li, Y., Feng, X., Lin, H., Huang, Z., Zheng, J., Shen, H., Zhu, L., Wang, C., Ye, J., and Yang, X.: Temperature-Dependent Evaporative Anthropogenic VOC Emissions Significantly Exacerbate Regional Ozone Pollution, Environ. Sci. Technol., 58, 5430–5441, https://doi.org/10.1021/acs.est.3c09122, 2024.

Wærsted, E. G., Sundvor, I., Denby, B. R., and Mu, Q.: Quantification of temperature dependence of NOx emissions from road traffic in Norway using air quality modelling and monitoring data, Atmos. Environ.: X, 13, 100 160, https://doi.org/10.1016/j.aeaoa.2022.100160, 2022.

Yan, K., Wang, J., Peng, R., Yang, K., Chen, X., Yin, G., Dong, J., Weiss, M., Pu, J., and Myneni, R. B.: HiQ-LAI: a high-quality reprocessed MODIS leaf area index dataset with better spatiotemporal consistency from 2000 to 2022, Earth Syst. Sci. Data, 16, 1601–1622, https://doi.org/10.5194/essd-16-1601-2024, 2024.

Yan, X., Ohara, T., and Akimoto, H.: Statistical modeling of global soil NOx emissions, Glob. Biogeochem. Cycles, 19, GB3019, https://doi.org/10.1029/2004GB002276, 2005.

Yienger, J. J. and Levy, H. I.: Empirical model of global soil-biogenic NOx emissions, J. Geophys. Res. Atmos., 100, 11 447–11 464, https://doi.org/10.1029/95JD00370, 1995.

Yuan, H., Dai, Y., Xiao, Z., Ji, D., and Shangguan, W.: Reprocessing the MODIS Leaf Area Index products for land surface and climate modelling, Remote Sens. Environ., 115, 1171–1187, https://doi.org/10.1016/j.rse.2011.01.001, 2011.

Zeng, G., Pyle, J. A., and Young, P. J.: Impact of climate change on tropospheric ozone and its global budgets, Atmos. Chem. Phys., 8, 369–387, https://doi.org/10.5194/acp-8-369-2008, 2008.

https://doi.org/10.5194/egusphere-2026-4644
Preprint. Discussion started: 9 September 2026

Zhu, Z., Piao, S., Myneni, R. B., Huang, M., Zeng, Z., Canadell, J. G., Ciais, P., Sitch, S., Friedlingstein, P., Arneth, A., Cao, C., Cheng, L., Kato, E., Koven, C., Li, Y., Lian, X., Liu, Y., Liu, R., Mao, J., Pan, Y., Peng, S., Peñuelas, J., Poulter, B., Pugh, T. A. M., Stocker, B. D., Viovy, N., Wang, X., Wang, Y., Xiao, Z., Yang, H., Zaehle, S., and Zeng, N.: Greening of the Earth and its drivers, Nat. Clim. Change., 6, 791–795, https://doi.org/10.1038/nclimate3004, 2016.